



UNIVERSITY OF LEEDS

This is a repository copy of *Influence of Seabed Morphology and Substrate Composition On Mass-Transport Flow Processes and Pathways: Insights From the Magdalena Fan, Offshore Colombia*.

White Rose Research Online URL for this paper:
<http://eprints.whiterose.ac.uk/115330/>

Version: Accepted Version

Article:

Ortiz-Karpf, A, Hodgson, DM orcid.org/0000-0003-3711-635X, Jackson, CA-L et al. (1 more author) (2017) Influence of Seabed Morphology and Substrate Composition On Mass-Transport Flow Processes and Pathways: Insights From the Magdalena Fan, Offshore Colombia. *Journal of Sedimentary Research*, 87 (3). pp. 189-209. ISSN 1527-1404

<https://doi.org/10.2110/jsr.2017.10>

(c) 2017 by the SEPM Society for Sedimentary Geology. This is an author produced version of a paper published in the *Journal of Sedimentary Research*. Uploaded in accordance with the publisher's self-archiving policy.

Reuse

Unless indicated otherwise, fulltext items are protected by copyright with all rights reserved. The copyright exception in section 29 of the Copyright, Designs and Patents Act 1988 allows the making of a single copy solely for the purpose of non-commercial research or private study within the limits of fair dealing. The publisher or other rights-holder may allow further reproduction and re-use of this version - refer to the White Rose Research Online record for this item. Where records identify the publisher as the copyright holder, users can verify any specific terms of use on the publisher's website.

Takedown

If you consider content in White Rose Research Online to be in breach of UK law, please notify us by emailing eprints@whiterose.ac.uk including the URL of the record and the reason for the withdrawal request.



eprints@whiterose.ac.uk
<https://eprints.whiterose.ac.uk/>

**INFLUENCE OF SEABED MORPHOLOGY AND SUBSTRATE COMPOSITION ON MASS-
TRANSPORT FLOW PROCESSES AND PATHWAYS: INSIGHTS FROM THE
MAGDALENA FAN, OFFSHORE COLOMBIA**

Running title: Influence of bathymetry and substrate on MTCs

**ANDREA ORTIZ-KARPF¹, DAVID M. HODGSON¹, CHRISTOPHER A.-L.
JACKSON², WILLIAM .D. McCAFFREY¹**

¹School of Earth and Environment, University of Leeds, Leeds LS2 9JT, UK

² Basins Research Group (BRG), Department of Earth Science and Engineering, Imperial
College, Prince Consort Road, London, SW7 2BP, UK

eealok@leeds.ac.uk

Key words: Mass-transport complexes (MTCs), debris flows, mass flows, Magdalena Fan,
deep water

June 2016

**INFLUENCE OF SEABED MORPHOLOGY AND SUBSTRATE COMPOSITION ON MASS-
TRANSPORT FLOW PROCESSES AND PATHWAYS: INSIGHTS FROM THE
MAGDALENA FAN, OFFSHORE COLOMBIA**

ANDREA ORTIZ-KARPF¹, DAVID M. HODGSON¹, CHRISTOPHER A.-L. JACKSON², AND
WILLIAM D. MCCAFFREY¹

¹ *School of Earth and Environment, University of Leeds, Leeds LS2 9JT, U.K.*

² *Basins Research Group (BRG), Department of Earth Science and Engineering, Imperial
College, Prince Consort Road, London, SW7 2BP, U.K.*

Email: eealok@leeds.ac.uk

ABSTRACT

Although the effects of interactions between turbidity currents and the seabed have been widely studied, the roles of substrate and bathymetry on the emplacement of mass-transport complexes (MTCs) remain poorly constrained. This study investigates the effect of bathymetric variability and substrate heterogeneity on the distribution, morphology, and internal characteristics of nine MTCs imaged within a 3D seismic volume in the southern Magdalena Fan, offshore Colombia. The MTCs overlie substrate units composed mainly of channel-levee-complex sets, with subsidiary deposits of MTCs. MTC dispersal was influenced by tectonic relief, associated with a thin-skinned, deep-water fold-and-thrust belt, and by depositional relief, associated with the underlying channel-levee-complex sets; it was the former that exerted the first-order control on the location of mass-transport pathways. Channel-levee-complex sets channelized, diverted, or blocked mass flows, with the style of response largely controlled by their orientation with respect to the direction of the incoming flow and by the height of the levees with respect to flow thickness. MTC erosion can be relatively deep above channel-fill deposits, whereas more subtle erosional morphologies are

observed above adjacent levee units. In the largest MTC, the distribution of the seismic facies is well imaged, being influenced by the underlying bathymetry, with internal horizontal contraction occurring updip of bathymetric highs, erosion and bypass predominating above higher gradient slopes, and increased disaggregation characterizing the margins. Hence, bathymetric irregularities and substrate heterogeneity together influence the pathways, geometries, and internal characteristics of MTCs, which could in turn influence flow rheology, runout distances, the presence and continuity of underlying reservoirs, and the capacity of MTCs to act as either hydrocarbon seals or reservoirs.

INTRODUCTION

Mass-transport complexes (*sensu* Weimer and Shipp 2004) comprise the products of submarine mass movements, including slides, slumps, and debris flows. The basal surfaces of MTCs can be defined by deep and widespread incision (e.g., Weimer and Slatt 2007; Posamentier and Martinsen 2011), with material entrained through erosion of the substrate along the path of the flow accounting for up to 40-50% of the total deposit volume (e.g., Prior et al. 1984; Gee et al. 2006; Lamarche et al. 2008; Joanne et al. 2013). The morphology of an MTC basal surface depends on the capacity of the flow to erode, which in turn depends on the characteristics of the flow and of the slope over which it propagates (Dykstra et al. 2011; Iverson 2012; Day et al. 2015).

Simplified MTC depositional models are useful in conveying the key characteristics of their bounding surfaces and internal character (e.g., Prior et al. 1984; Weimer and Slatt 2004; Frey-Martinez et al. 2005; Bull et al. 2009). However, these models assume a layered, low-relief, homogeneous substrate, which typically does not adequately capture the bathymetrically complex, heterogeneous substrates encountered in many deep-water settings. For example, the slope in some active and passive continental margins is complicated by tectonic, gravity, and salt-driven structures (e.g., Steffens et al. 2003; Moscardelli et al. 2006; Heniö and Davies 2006; Gee et al. 2007; Gamboa et al. 2010; Clark and Cartwright 2009, 2012; Vinnels et al. 2010). In areas lacking major structures,

depositional relief associated with channel-levee complexes, MTCs and/or contourites can produce bathymetric irregularities that can influence the flows that propagate above them (e.g., Nakajima et al. 1998; Migeon et al. 2001; Piper and Normark 2001; Skene et al. 2002; Frey-Martinez et al. 2006; Jackson and Johnson 2009; Alves 2010; Kneller et al. 2015; Ducassou et al. 2015; Ortiz-Karpf et al. 2015). Moreover, differences in the compositional and textural characteristics of the various deep-water architectural elements result in lithological heterogeneities, which can make them variably susceptible to erosion and entrainment. Entrainment of different types of substrate can modify the rheology and structure of submarine sediment gravity flows and, therefore, the distribution and structure of the resulting deposits (e.g., Iverson 1997, 2012; Dykstra et al. 2011; Joanne et al. 2013). The heterogeneity resulting from entrainment of material with different compositions and clast sizes can potentially affect the ability of MTCs to act as hydrocarbon seals or reservoirs (e.g., Gamboa et al. 2010; Meckel [III] 2011; Meckel [III] et al. 2011; Omosanya and Alves 2013; Alves et al. 2014; Cardona et al. 2016).

This study uses a 3D seismic reflection volume located in the southern Magdalena Fan, offshore Colombia to investigate the effect of bathymetric relief and substrate heterogeneities on the dispersal patterns, distribution, geometries, and seismic facies of several Pleistocene MTCs. Here, tectonic structures formed due to thin-skinned shortening; multiple stacked channel-levee-complex sets combine to form a complicated slope upon which several highly erosional MTCs were transported and emplaced (Ortiz-Karpf et al. 2015, 2016). The geological setting and the high seismic resolution at shallow stratigraphic levels make it an ideal dataset to study MTC-substrate interactions in detail.

DATA

This study uses a post-stack depth-migrated (PSDM) seismic survey that covers an area of 1900 km² and which has a bin spacing of 12.5 m x 12.5 m. This study focuses on a 1-km-thick stratigraphic succession immediately below the seabed. At this depth the dominant frequency is 30 Hz and the assumed sediment velocity is 1900 m/s, yielding a vertical and

horizontal resolution of c. 10-15 m and c. 15 m respectively (Ortiz-Karpf et al. 2015, 2016). The seabed is defined by a positive reflection represented by a black horizon in the seismic images shown herein. A few wells lie NE of the study area, but they were not available for this study.

GEOLOGICAL SETTING

The Magdalena Fan is located in the Caribbean Sea, off the northern coast of Colombia, South America (Fig. 1A). This is a tectonically active margin, where the Caribbean Plate subducts obliquely beneath the South American Plate, resulting in the development of imbricate fold-and-thrust belts (Duque-Caro 1979; Pindell, 1994; Meschede and Frisch 1998; Cediel et al. 2003; Pindell and Kennan 2009). The youngest fold-and-thrust belt is the Sinú Fold Belt, which is located offshore and has experienced episodic growth since the Middle to Late Miocene (Cediel et al. 2003; Martinez et al. 2015), propagating sequentially to the north (Bernal-Olaya 2015; Martinez et al. 2015). The Sinú Fold Belt is divided into the Southern and Northern Sinú Fold belts, with subdued deformation and relief characterizing the area between the two segments (Fig. 1B). The Magdalena Fan has evolved in the central, relatively undeformed area, since the Late Miocene (Duque-Caro 1979, 1984; Kolla and Buffler 1984; Breen 1989; Romero-Otero 2009; Martinez et al. 2015) (Fig. 1B).

The study area is defined by the outline of the three-dimensional seismic volume, which is located in the northern tip of the Southern Sinú Fold Belt (Fig. 1B). It images two large anticlines, referred to as the *Downdip Anticline* and *Updip Anticline*, which are separated by a syncline (cf. Ortiz-Karpf et al. 2016; Fig. 2B-D). The Downdip Anticline is composed of two segments separated by a saddle (Fig. 2B-D). The southern segment is thrust-cored and asymmetric, with its steepest flank dipping to the NW (Fig. 2B, D). The northern domain is broader, is more symmetric, and is not faulted (Fig. 2C). The Updip Anticline is asymmetric and thrust-cored, with a steep, NW-verging frontal limb (Fig. 2D). To the west of these tectonic structures, the seabed is dominated by compensationally stacked channel-levee-complex sets that are c. 100-200 m high at the external levee crests (Fig. 2C-E). The

primary depositional geometry of the channel-levee-complex sets is sometimes modified by sediment waves and MTCs (Romero-Otero 2009).

METHODOLOGY

Using the same seismic survey as used here, Ortiz-Karpf et al. (2015) define seven seismic facies, and interpret a number of sedimentary sub-environments (i.e. channel fill, levees, lobes, and MTCs) arranged into seven mappable seismic units. Seismic Unit D (*sensu* Ortiz-Karpf et al. 2015) is located c. 300-500 m below the seabed, and comprises coalesced MTCs that overlie a composite basal erosion surface (Fig. 3). Ortiz-Karpf et al. (2016), studied a total of nine MTCs, five that are within Unit D and four that underlie it (Fig. 3B). In this study, using the seismic facies classification defined by Ortiz-Karpf et al (2015), and mapping key, laterally continuous seismic-stratigraphic surfaces, six seismic units that underlie the nine MTCs investigated by Ortiz-Karpf et al. (2016) were also defined (Fig. 3B). The relative chronology of the substrate units was established through their seismic-stratigraphic relationships (e.g., onlap, downlap, erosional truncation).

A separate seismic facies classification was defined for the largest MTC (MTC C1 cf. Ortiz-Karpf et al. 2016) in order to capture its internal heterogeneity (Table 1). This approach is based on previous studies that have used lithologically calibrated 3D seismic (e.g., Alves et al. 2014) and seismic forward modelling (Dykstra et al. 2011) to: i) demonstrate that the internal deformation and coherency of mass-transport deposits is portrayed accurately by the lateral continuity of the seismic reflections; and 2) validate that seismic attributes such as amplitude, dip, and variance can be used to infer lateral heterogeneity. Using this approach we identify five MTC seismic facies based on the amplitude, variance, and lateral continuity of the reflections (see Table 1). Facies 1 to 4 are composed of low-to-variable amplitude, discontinuous to semicontinuous reflections and are interpreted as debrites (cf. Posamentier and Kolla 2003; Gamboa et al. 2011; Olafiranye et al. 2013). Variations in the continuity, amplitude, and orientation of the reflections are interpreted to indicate changes in the degree of disaggregation of the material and internal deformation (cf. Alves et al. 2014). Seismic

facies 1, which is composed of low-amplitude, discontinuous, chaotic reflections, is interpreted to contain highly disaggregated material (Table 1B and C); seismic facies 2 is composed of semicontinuous, folded reflections with unclear fold vergence and is interpreted to contain partially disaggregated material (Table 1D and E); seismic facies 3 is characterized by semicontinuous, thrust and folded reflections that form thrust and fold systems (*sensu* Bull et al. 2009) and is interpreted to contain more coherent and less disaggregated material than that of facies 1 and 2 (Table 1E). Seismic facies 4 is composed of low-amplitude, homogeneous packages with few internal reflections and is interpreted as mud-prone debrites (cf. Posamentier and Kolla 2003; Table 1 F and G); and seismic facies 5, is composed of discrete packages of coherent, parallel, generally folded reflections contained in a matrix composed mainly of seismic facies 1 and 2, and is interpreted as megaclasts (cf. McGilvery et al. 2004; Bull et al. 2009; Frey-Martinez 2010; Gamboa et al. 2011; Posamentier and Martinsen 2011; Olafiranye et al. 2013; Jackson 2011; Alves 2015) (Table 1A and B).

In order to investigate the lateral and vertical distribution of the MTC seismic facies, the interval defined by the top and base surfaces of the largest MTC was divided into four proportional slices using pseudo-horizons, and interval attribute extractions were generated (see approach outlined by Zeng et al. 1998). Variance and RMS amplitude were found to be the most useful attributes to define the limits between seismic facies, and they were integrated with observations from cross sections and depth slices in amplitude, variance, and impedance volumes to generate an MTC seismic facies map.

SEISMIC STRATIGRAPHY

Pre-MTC Stratigraphy

The MTCs in the interval of interest erosionally overlie remnants of older MTCs and channel-levee-complex sets that are interpreted to have been active at different times. The external levees are defined by low-amplitude, parallel internal reflections that downlap onto

underlying strata (Fig. 3B). The channel fill is composed of stacked packages of relatively high-amplitude discontinuous reflections (Fig. 3B). In order to assess the importance of possible variations in substrate properties, six seismic units (Units I-VI) were defined by mapping the most laterally extensive channel-levee-complex sets and establishing their relative chronology based on seismic-stratigraphic relationships (Figs. 4 and 5). Figure 4 illustrates the stratigraphic relationship between the various substrate units and the overlying MTCs. Figure 5 shows the spatial distribution of the substrate units directly underlying the MTCs (Fig. 5A), their spatial relationship with respect to the overlying MTCs (Fig. 5B), and the location and overall trend of their channel axes (Fig. 5C). Units I and IV are developed in the south of the study area (Fig. 5A). Unit I is folded into the southern Downdip Anticline, and its channel axis trends W (Fig. 5A and C). Unit IV is preserved only west of the southern Downdip Anticline, and its axis is almost entirely eroded by subsequent MTCs (Fig. 4). Units II, III, V, and VI occur in the NE of the study area and are folded into the northern Downdip Anticline (Fig. 5A). Their channel axes trend WNW, with the axes of Units V and VI being partially eroded below the overlying MTCs (Fig. 4).

MTCs

The nomenclature of the nine MTCs defined by Ortiz-Karpf et al (2016) is based on their location in the study area. MTCs S1 to S6 are located towards the SW, basinwards of the southern Downdip Anticline (Fig. 3). MTC C1 is located towards the center of the study area, crosscutting the Downdip Anticline at the saddle developed between the southern and northern segments (Fig. 3A). MTCs N1 and N2 are located towards the NE and traverse the northern Downdip Anticline (Fig. 3A). Five of the MTCs (S5, S6, C1, N1, and N2) form part of Unit D as defined by Ortiz-Karpf et al. (2015) and four underlie it (S1-S4; Fig. 3B).

MTCs S1-S6--- S1-S6 are elongate in a NE-SW direction (Fig. 3A). S1-S5 extend beyond the southern limit of the seismic survey (Fig. 3A). To the NW S1-S3 are bounded by southeastern levee of Unit I (Figs. 3B, 4A, and 6A), and S4-S6 by the northwestern levee of Unit IV (Figs. 3B, 5B and 6A). To the SE, S1-S5 and S6 are bounded by the southern

Downdip Anticline (Fig. 6A), while S4 is limited by the northeastern levee of Unit I (Figs. 3B, 4A, and 6A).

Ortiz-Karpf et al. (2016) interpret S5 to have been emplaced by NNE-directed flows based on the orientation of grooves in the basal surface and on the orientation and vergence of folds contained within megaclasts. Based on the orientation of the lateral margins of S1-S3, the NE-SW alignment of megaclasts, and the northern onlap against the southeastern levee of Unit I, Ortiz-Karpf et al. (2016) also infer S1-S3 to have been emplaced by NNE-directed flows. Contrary to MTCs S1-S3 and S5, S6 is interpreted to have been sourced from the NE and emplaced by a SW-directed flow because it widens to the SW and terminates downdip against protrusions along the top of S5 (Ortiz-Karpf et al. 2016; Fig. 3B). The provenance of S4 is uncertain because it continues beyond the southern limit of the dataset, and its northeastern portion was eroded by S6 and C1 (Ortiz-Karpf et al. 2016; Fig. 3B).

The southern levee of Unit I, which is overlapped by S1-S3 (Fig. 4A) is orientated WSW, which is highly oblique to the interpreted NNE flow direction of S1-S3 (Fig. 5B). Unit I is hence interpreted to have constituted a barrier that restricted their down-flow extent. S4 overlies the channel axis of Unit I (Fig. 4A) and follows its overall trend (Ortiz-Karpf et al. 2016) (Fig. 5B); it is therefore interpreted to have exploited the underlying channel. It is possible that S6 was confined between the southern Downdip Anticline and Unit IV (Fig. 6A), but erosion of Unit IV makes it difficult to infer its original depositional geometry.

MTC C1--- MTC C1 is the most laterally extensive MTC, extending beyond the eastern and western limits of the dataset (Fig 3A). Based on the presence of arcuate scarps in the present-day shelf break, Ortiz-Karpf et al. (2016) interpret C1 was sourced at or close to the shelfbreak. C1 trends along the syncline between the Updip and Downdip anticlines and across the Downdip Anticline into the basin low (Fig. 7A). The basal surface is erosional and covers an area of c. 400 km² within the study area. The top surface is characterized by irregular protrusions (Fig. 7B), and the deposit covers an area of c. 300 km² within the dataset. C1 was emplaced above a bathymetrically complex seabed and eroded several

stratigraphic units (Figs. 4 and 5B); this enables the investigation of the relationship between the geometry of the basal surface and the distribution of the seismic facies, with the characteristics of the underlying substrate. The morphology of the basal surface, its geographic relationship with the substrate units, and the distribution of the seismic facies are hence described below from E to W, starting from the syncline, progressing downdip across the Downdip Anticline, and finally into the basin low (see Fig. 8).

In the syncline (Fig. 8C), the basal erosion surface of C1 is c. 6 km wide and up to c. 600 m deep. The overlying MTC is, however, only c. 100-200 m thick, indicating that the erosional relief in this area is severely underfilled (cf. “evacuated morphology” of Eggenhuisen et al. 2010) (Fig. 8C). The lateral margins of C1 are stepped, being characterized by relatively steep slopes (c. 24°). The eastern margin of C1 is defined by the frontal flank of the Updip Anticline, whereas the western margin is defined by the back limb of the northern Downdip Anticline, which is composed largely of the southern levees of units II, V, and VI (Fig. 8C). Along the syncline, C1 locally overlies the channel axis of Unit II (Fig. 5B). In general, the basal surface is relatively steep above Units V and VI and relatively flat above Unit II (Fig. 8C and D). In the back limb of the northern Downdip Anticline, there is a NW-trending, narrow erosional trough that potentially links the basal surface of C1 with that of N1 and N2 (Fig. 7A, C, and D). This trough incises through the external levees of Unit VI and partially erodes Unit V (Fig. 7C). The channel axis of Unit VI is not present, and presumably was eroded (Fig. 7C). The erosion surface across this trough is overlain by a thin (c. 50 m) package of debrites (Fig. 7C and D). In the syncline the deposit is thickest towards the eastern limit of the dataset (c. 200 m), where imbricate thrust and fold systems (facies 3) develop (Fig. 9A and D). Thrust planes dip to the NE (Fig. 10B), suggesting emplacement by an overall SW-trending flow. To the SW, the thrust and fold system transitions to facies 2, which is on average 100 m thick and, despite being folded, lacks systematic faulting (Fig. 9A and D). Updip of the saddle between the southern and northern segments of the Downdip Anticline, a W-trending basal erosion surface incises through the entire thickness of facies 2.

This erosion surface is filled with low-amplitude debrites (Facies 4; Fig. 9D) and is interpreted to be younger than C1. The northwestern margin of the syncline and part of the southeastern margin contain low-amplitude, chaotic debrites (Facies 1; Fig. 9D).

C1 traverses the Downdip Anticline at the saddle between the southern and northern segments (Fig. 8A). Across the Downdip Anticline, the basal surface progressively narrows to from c. 8 to 5 km (Fig. 8D and E), and the axial slope steepens from c. 2° to 6°. Here, the southern lateral scarp of C1 is composed of units I and IV, and the northern scarp by units II, V, and VI (Fig. 8D-G). The northern lateral scarp tends to be steeper across Unit VI, which is affected by more normal faults, than across Unit II, which contains fewer faults and is less reflective (Figs. 5D and 8D). The thickness of the deposit decreases abruptly to < 50 m (Fig. 9A) across the anticline, where it is composed of megaclasts (facies 5) contained in a thin (< 50 m) chaotic matrix (Facies 1; Fig. 9D). Most megaclasts are roughly aligned parallel to the lateral margins (Fig. 9C and D).

Basinwards of the Downdip Anticline (Figs. 8E-G), the slopes of the lateral walls and the erosional relief of the basal surface progressively decrease. The basal surface also widens, reaching c. 10 km in width towards the western limit of the dataset, where it is completely filled by MTC material (Fig. 8G). The southern margin of C1 is composed of units I and IV (Fig. 8F), whereas the northern margin is composed by units II, V and VI (Fig. 8E). The basal surface of C1 tends to be steeper across units V and VI than across Unit II (Figs. 8E and F); farther downdip it is bounded to the NW by Unit III (Fig. 8G). At the toe of the Downdip Anticline, the deposit thickens progressively to > 150 m (Fig. 9A) and is composed of imbricate thrust and fold systems (Facies 3; Figs. 9 and 10). The thrusts dip ESE and become more closely spaced and steeper basinward (Fig. 10B), supporting interpretation of a WNW emplacement direction. The thrust and fold system terminates against a landward-dipping ramp developed along the basal erosion surface; at this location, the deposit thins from c. 150 m to c. 100 m. Downdip of this location, C1 is composed of semicontinuous, folded reflections with no systematic faulting (Facies 2; Figs. 9 and 10). Towards its lateral

margins, the deposit thins to < 50 m (Fig. 9A) and is composed mainly of debrites (facies 1) and megaclasts (facies 5; Figs. 9 and 11B).

The megaclasts in C1 are up to c. 0.6 km² in map view and occur in facies 1-3 (Fig. 10). The length of the longest axis of the megaclasts in C1 ranges from 0.22 to 1.6 km, and 70% of the megaclasts have map-view aspect ratios between 1 and 2 (Fig. 12B). Megaclasts are 20 to 280 m thick (Fig. 12C). Internally, most megaclasts are characterized by low-amplitude, folded reflections (e.g., Fig. 11). In some cases, the internal reflections are contorted or chaotic and, in a few cases, they are either reflection-free or contain subparallel, subhorizontal reflections (Fig. 11B and Table 1). Megaclasts are more abundant basinward of the Downdip Anticline, where they are concentrated towards the southern and northwestern margins (Figs. 9D and 12A). Some of the largest and more deformed megaclasts occur basinward of the Downdip Anticline, in the northwestern margin (Fig. 12), where they overlie the southern external channel-levee of Unit III (Fig. 13B). Along the opposite margin, megaclasts with plan-view areas of c. 0.4 km² are clustered above areas of increased incision of the basal erosional surface above Unit IV (Fig. 13B). 30% of the megaclasts are located in the syncline and across the saddle between the northern and southern segments of the Downdip Anticline (Figs. 12A).

A series of lineaments are developed on the basal surface of MTC C1. They are particularly well imaged in variance extractions, where they are oriented subparallel to the lateral margins of the basal surface (Ortiz-Karpf et al. 2015) (Fig 13A). In cross section the lineaments appear as V-shaped erosional scours that have a similar appearance irrespective of the underlying substrate unit (Fig. 13B). They are interpreted as “grooves” (*sensu* Bull et al. 2009) formed by megaclasts transported at the base of the flow (cf. Posamentier and Kolla, 2003; Bull et al. 2009; Sobiesiak et al. 2016). The orientation and downslope divergence of the grooves, together with the overall morphology of the basal surface and the vergence of the faults in the imbricate thrust and fold systems, are used to infer the MTC flow direction, which, in this case, is interpreted as being: (i) NW-directed towards the

eastern limit of the dataset; (ii) southwestward in the syncline; (iii) NW-directed across and directly basinward of the Downdip Anticline, and (iv) SW-directed towards the western limit of the dataset (Fig. 13A).

MTCs N1 and N2--- MTCs N1 and N2 overlie a composite, SW-trending erosion surface that overlies units V and VI above the northern Downdip Anticline (Fig. 3), and Unit III towards the western limit of the seismic survey (Fig. 5A). Based on the morphology of the basal surface, which is parallel to the underlying channel-levee-complex sets (Fig. 5C), N1 and N2 are interpreted to have been emplaced by SW-directed flows (Ortiz-Karpf et al. 2016). Because the composite erosion surface is located downdip of scarps on the present shelf break, Ortiz-Karpf et al. (2016) interpreted N1 and N2 to have been sourced from the outer shelf or upper slope. On the western limb of the Downdip Anticline, the composite basal erosion surface of N1 and N2 incised more deeply into the channel axis of Unit V than the flanking levees and the channel axis of Unit VI was eroded completely (Fig. 6D). Basinwards of the northern Downdip Anticline, the channel axes of both units are absent (Fig. 5C) and N1 overlies a debrite with a deep erosional base (Fig. 6C). The position of the underlying debrite is interpreted to roughly mark the position of the eroded channel axes of units V and VI.

DISCUSSION

Bathymetric and Substrate Controls on Flow Pathways and Deposit Geometry

Influence of Structural Relief--- The most prominent bathymetric features in the study area are the tectonic structures, which were a principal control on the dispersal and ultimate distribution of the MTCs. The change in overall flow direction of C1, from NW towards the eastern limit of the dataset, to SW in the syncline, was driven by the presence of the northern Downdip Anticline, which forced the flow to follow the trend of the synclinal hinge (Fig. 13A). The MTC traversed the Downdip Anticline at the saddle between the southern and northern segments, indicating that the location of the erosion surface across

the anticline was also likely controlled by the syndepositional structural configuration. This concurs with previous studies that have found structural relief to control the distribution and geometry of MTCs, with MTCs being laterally confined by tectonic structures, ponded in piggy-back or salt-withdrawal basins (e.g., Vinnels et al. 2010; Jones et al. 2012; Alfaro and Holz 2014) or blocked against structural highs (Jones et al. 2012).

Influence of Depositional Relief--- Basinward of the anticlines, the depositional relief of the channel-levee-complex sets constituted the main bathymetric perturbations. By comparison with similar channel-levee-complex sets on the present seabed, these buried systems could have been c. 100-200 m high at the external levee crests (e.g., Fig. 6A-C). The orientation of the channel-levee-complex sets with respect to the emplacement direction of the mass flows determined the MTC flow pathways and depositional geometries. The flow direction of MTCs N1 and N2 was subparallel to the orientation of the underlying channel-levee-complex sets in units V and VI (Fig. 3B and C), and N1 and N2 are therefore interpreted to have exploited the underlying channel conduits. Similar interactions are observed offshore Trinidad, where some MTCs are focused along underlying canyons (Moscardelli et al. 2006). To the west of the Downdip Anticline, MTC C1 was also parallel to the underlying channel-levee-complex sets. Although erosion of Unit IV obscures its original depositional geometry, it seems likely that C1 was emplaced along the bathymetric low between the northern levee of Unit IV and the southern levee of units V and VI (Fig. 4). In the Magdalena Fan, north of the present study area, Romero et al. (2010) also document MTCs focused along interchannel lows. Farther downdip, MTC C1 was deflected to the SW by the southern levee of Unit III, which was oriented oblique to the propagation direction of C1 (Fig. 5). A similar deflection of an MTC by the external levee of a channel-levee-complex set is documented by Deptuck et al. (2007) in the Niger Delta slope.

In contrast to MTCs C1, N1, and N2, the propagation direction of MTCs S1-S5, which is interpreted as NNE, was highly oblique to the WSW-trending underlying channel-levee-complex set in Unit I (Fig. 5B). Due to its depositional relief, Unit I constituted a barrier that

limited the down-flow extent of MTCs S1-S5. In summary, the depositional relief of channel-levee-complex sets can focus, deflect, or block mass flows.

Differential Erosion--- Erosion generated at the bases of MTCs is sometimes greater above channel axes in comparison to the surrounding levees, with this relationship being observed: i) in the western flank of the northern Dwindip Anticline, where deeper erosion under the composite basal surface of N1 and N2 is observed above the channel axis of Unit V (Fig. 6D); ii) west of the northern Dwindip Anticline, where the channel axes of units V and VI have been completely eroded by N1 and N2, whereas flanking levees have been preserved (Figs. 5A, C, and 6C); and iii) in the erosional trough that connects the basal erosion surface of C1 to the composite erosion surface of N1 and N2, where it occurs between the levees of unit V and VI and the channel axis is absent (Fig. 7A, C, and D). These observations suggest that channel-fill deposits were preferentially eroded during the emplacement of the MTCs. This had an associated effect on the morphology of the basal erosion surface and local sediment flow pathways by determining the location of the trough connecting C1 and N1/N2 (Fig. 7).

Preferential erosion of the channel axis can be explained by a number of mechanisms. First, the presence of bathymetric lows above underfilled channel axes could have focused subsequent MTCs. This is considered unlikely because most of these channel-levee complexes were inactive and buried at the time of MTC emplacement, meaning that any underfilled relief would have been healed by subsequent sedimentation. A further possibility is the development of postdepositional bathymetric lows above channel axes due to differential compaction of the channel-fill sediments with respect to the levees, resulting from lithological differences between channel-fill and levee deposits (Mayall et al. 2006). Previous studies show that the fills of slope channel-levee complexes commonly comprise coarser-grained, heterolithic material (e.g., Mayall et al. 2006; Babonneau et al. 2010; Hodgson et al. 2011; Hubbard et al. 2014; Jobe et al. 2015), whereas levees generally contain fine-grained, clay-rich material (e.g., Babonneau et al. 2010; Kane and Hodgson 2011; Morris et al. 2014;

Hansen et al. 2015). These characteristics are reflected in the amplitude and continuity of the seismic reflections, with channel-fill deposits being characterized by variable amplitude, discontinuous reflections, and levees containing low-amplitude parallel, continuous reflections (e.g., Fig. 3B; e.g., Pirmez et al. 1997; Deptuck et al. 2003; Nakajima and Kneller 2013). These lithological differences can result in variable shear strengths and yield different susceptibilities to erosion, potentially explaining preferential erosion of channel-fill sediments. The electrochemical forces between clay particles lead to rapid consolidation and the development of shear strength upon sedimentation (e.g., Mehta et al. 1989). Thus clay-rich levees could be more resistant to erosion than channel-fill sediments with lesser clay content. Also, sandy sediments have a higher tendency to undergo liquefaction. Liquefaction results from pore-pressure buildup within the boundary layer as it is loaded by the overriding flow (e.g., Butler and Tavarnelli 2006; Iverson 2012). If channel-fill deposits contain sand-sized particles, they could hold a higher pore-fluid volume and be more susceptible to liquefaction and entrainment. This process is invoked by Georgiopoulou et. al. (2010) to explain erosion and entrainment of a volcanoclastic sand layer underlying the Sahara Slide offshore NW Africa. Also, Joanne et al. (2013) calculate that 40% of the volume of the Matakaoa debris flow located offshore New Zealand, corresponds to entrained material and propose that the high entrainment rates relate to the sandy nature of the substrate, which makes it prone to MTC erosion. It is plausible, therefore, that the deeper MTC erosion above channel axes documented in this study is a consequence of lithological variations between channel-fill and levee deposits, through liquefaction of sandy-channel fills and/or the cohesive levees being more resistant to erosion.

If abandoned before fully filling, the upper parts of submarine channels can also be mud-prone (cf. Mayall et al. 2006), thus it is impossible to determine the original composition of material now eroded from beneath the MTCs. Although the lack of lithological calibration and the widespread erosion by the MTCs makes it impossible to determine the specific cause of preferential erosion of channel-fill deposits, the observed relationship merits further

investigation because it suggests that substrate heterogeneities are an important control on MTC erosion and on the preservation potential of various deep-water architectural elements.

Subtle changes in the morphology of the basal surfaces across levees could also be attributed to substrate heterogeneity. For example, the basal erosion surface of C1 tends to be steeper across the external levees of Unit VI and flatter above the levees of Unit II (Figs. 6D, 8C, and D). This difference coincides with variations in the seismic character and deformation of the substrate units. Unit VI levees display higher amplitudes and more faulting than the levees of Unit II, which could reflect differences in the mechanical properties of the levees due to variations in the compositional and textural character of levees deposited by different channels, as well as variable degrees of compaction and lithification resulting from different burial histories.

Types of Interaction between MTCs and Channel-Levee-Complex Sets--- Based on the observed influence of seabed morphology and the composition of the MTCs, four generic types of interaction between mass flows and the underlying channel-levee-complex sets are proposed (Figure 14). These are end-member scenarios, and intermediate situations are likely to occur during MTC emplacement.

Type 1: MTCs Overlie and Exploit Underlying Channel Conduits--- This occurs when the mass flow is parallel to an underlying channel-levee-complex set and is confined within its levees (Fig. 14). Due to erosion of channel-axis deposits, the mass flow is likely to become entrenched, preferentially entraining the channel-fill deposits and potentially increasing the sand content of the mass flow. The depth of erosion above the levees is likely to be lower than above the channel axis.

Type 2: MTCs Confined in Interchannel Lows--- Mass flows focused along interchannel lows may be entirely confined if the external levees are high relative to the thickness of the mass flow, eroding only the levees and preserving the adjacent channel axes (Fig. 14). The

morphology of the basal surface is likely to be influenced by variations in the properties of the underlying levees.

Type 3: MTCs Deflected by Levees--- The presence of channel-levee-complex sets oriented obliquely to the transport direction can cause the mass flow to be diverted away from the external levee, introducing a change in the overall flow direction (Fig. 14). If the height of a deflecting levee is greater than the thickness of the flow and associated flow runup, the channel axis is likely to be preserved. If the mass flow is able to erode and override the levee, it may become focused above the adjacent channel axis in a Type 1 interaction. Alternatively, the flow may become focused along the interchannel low following a Type 2 interaction (Fig. 14).

Type 4: MTCs Blocked by Levees--- When an underlying channel-levee-complex set is perpendicular or highly oblique to the flow direction and the height of the external levee exceeds the flow thickness, the levee can act as a barrier that blocks the mass flow and hinders further basinward transport and the erosion of the channel axis (Fig. 14).

The type of interaction between mass flows and the underlying channel-levee-complex sets can therefore control their flow pathways and influence the volume and type of substrate entrained. Dykstra et al. (2011) discuss the effect of substrate entrainment on the compositional and rheological evolution of mass flows and document shearing of sand from entrained megaclasts into the matrix of an MTC. They note that MTCs propagating over sandy substrates may become sandier downslope. Therefore, it is possible that debris flows above sandy channel axes may erode deeper, becoming entrenched and entraining sandy sediment. These debris flows could become less cohesive downslope and be transformed into hybrid flows or turbidity currents. Conversely, debrites propagating above muddy levees could cause less erosion and entrain muddy sediment, becoming more cohesive downslope and potentially freezing *en masse*. Understanding these different scenarios has an important application in prediction of flow pathways and runout distances. The type of interaction between mass flows and underlying channel-levee-complex sets has implications for the

presence and continuity of underlying hydrocarbon reservoirs. Channel axes oriented parallel or subparallel to the emplacement direction of mass flows may be more susceptible to erosion than those perpendicular or highly oblique, because the latter are shielded by their levees (types 3 and 4; Fig. 14).

Substrate and Bathymetric Controls on the Distribution of the Seismic Facies of C1.

The seismic facies distribution in C1 is interpreted to reflect the heterogeneity of the deposit. The various facies are interpreted to represent the degree of stratal disaggregation and internal deformation incurred during transport and emplacement. Here we discuss the effects of bathymetry on the flow processes and resulting deposit.

Distribution and Nature of the Megaclasts (Facies 5)--- Megaclasts in C1 vary in size, with their long axes ranging from 0.22 to 1.6 km and thicknesses ranging from 20 to 280 m (Fig. 12B and C). These megaclasts are comparable in size with those reported in similar seismic-based studies of Cretaceous MTCs in the Santos Basin, offshore Brazil (Jackson 2011) and Morocco (Lee et al. 2004; Dunlap et al. 2010). They are, however, comparatively small with respect to some Tertiary megaclasts reported offshore Brazil, which reach 5 km long and 350 m thick in the Santos basin (Jackson, 2011), and 4.5 km long and 500 m in the Espírito Santo Basin (Alves, 2010). Megaclasts in C1 are also significantly smaller than those reported in MTC S5, which are up to 4 km long and up to 300 m thick (Ortiz-Karpf et al. 2016). These variations in size could be related perhaps to different compositions, transport distances, and/or transport mechanisms.

The basal grooves at the base of C1 suggest that some megaclasts were transported for several kilometers (Fig. 15). There are multiple possible origins for the megaclasts. They may have been: i) derived from the original shelf-margin failure, ii) sourced from local collapse of the MTC lateral margins, iii) entrained through erosion of the Downtip Anticline, or iv) locally entrained, where found in clusters and within erosional scours.

More megaclasts are identified towards the MTC margins (Figs. 9 and 12A). Alves and Cartwright (2009) and Day et al. (2015) also noted that megaclasts concentrate at MTC margins in the Espírito Santo Basin offshore Brazil, and offshore Papua New Guinea, respectively. The concentration of megaclasts at the margins could be explained by increased friction at the base and margins of the upstepping basal erosion surface leading to local entrainment. The occurrence of large megaclasts clustered above the eroded external levee of Unit III along the northwestern margin of C1 (Figs. 11B and 15) could be attributed to local entrainment resulting from increased shear stress as the mass flow was deflected to the SW above the levee (Type 3 interaction; Fig. 14). Alternatively, the concentration of megaclasts at the MTC margins could be explained by dynamic grain-size segregation pushing larger particles towards the margins, a process which has been observed in subaerial debris flows (e.g., Major 1997; Johnson et al. 2012).

Occurrence of Low-Amplitude Discontinuous Reflections (Facies 1)--- Facies 1 is interpreted as debrites that comprise highly disaggregated material (Table 1). This facies occurs preferentially towards the margins of the deposit and across the DOWNDIP Anticline (Fig. 9). This observation is similar to that made by Alves and Cartwright (2009) and Gamboa et al. (2011), who document the occurrence of increasingly chaotic seismic facies in the thinner portions of MTCs offshore Brazil. The chaotic character of facies 1 could be explained by increased shear stress at the base of the flow, caused by the shallowing of the erosion surface, and by lateral shearing against the margins, which may cause increased mixing and disaggregation of the material.

Across the DOWNDIP Anticline facies 1 overlies a relatively smooth basinward-facing erosion surface that truncates the crest of the underlying structure (Fig. 11A). Here, facies 1 is thin (≤ 50 m) and is associated with aligned megaclasts (Fig. 9). Erosion could have been caused by the bypassing head of the flow, and the megaclasts could have been deposited by the predominantly bypassing body of the flow as a lag (Stevenson et al. 2015). The matrix could have been deposited later by a finer-grained and more disaggregated tail. Alternatively,

deposition may have occurred *en masse*, with the megaclasts and the matrix emplaced simultaneously.

Occurrence of Semicontinuous, Folded Reflections (Facies 2) and Imbricate Thrust and Fold Systems (Facies 3)--- Facies 2 and 3 occur predominantly in the central part of the deposit (Fig. 9). The abundance of systematically downdip-facing imbricate folds and thrusts in facies 3 suggests a higher degree of horizontal contraction with respect to facies 2, which comprises a broader range of fold styles and lacks associated thrusting (Table 1; Fig. 10). Thrust and fold systems tend to occur updip of bathymetric highs that constituted flow barriers. In the syncline, they develop updip of the back limb of the northern Downdip Anticline, which is interpreted to have deflected the flow to the SW (Fig. 9D). Basinward of the Downdip Anticline, they are found between the toe of the Downdip Anticline, where the slope decreases abruptly from c. 6° to c. 3°, and the levee of Unit III, which is interpreted to have deflected the flow to the SW in a Type 3 interaction (Figs. 9 and 14). The fold and thrust systems are interpreted as the response to flow deceleration and internal contraction against bathymetric highs. In a similar way, the development of imbricate thrusts and folds in an MTC offshore Trinidad is associated with lateral confinement of the mass flow by mud diapirs, which resulted in flow contraction (Moscardelli et al. 2006). Thus, comparable thrust and fold systems could develop in MTCs updip of either structural or depositional bathymetric highs that deflect or block the mass flows in type 3 or type 4 interactions (Fig. 14). The folds in facies 2 also indicate contraction, but the lack of a consistent sense of vergence suggest that these folds formed due to internal deformation resulting from simple shear against the basal surface, rather than due to abrupt deceleration resulting from downdip blockage or deflection. These folds could also represent a transition from the more coherent debrites (facies 3) to disaggregated debrites (facies 1; e.g., Shanmugam et al. 1994; Stow et al. 1996; Locat and Lee 2005; Strachan 2008; Omosanya and Alves 2013).

The characteristics of the flow at the time of emplacement are recorded in the seismic facies (e.g., Strachan 2008; Dykstra et al. 2011; Alves et al. 2014), resulting from the deformation, disaggregation, and mixing of the original failed mass, and entrainment of fluid and substrate (Shanmugam et al. 1994; Strachan 2008; Dykstra et al. 2011). The initial composition and texture of C1 would have been determined by the characteristics of the failed material. The main source area of C1 is interpreted to be located to the east of the study area, at or close to the shelf break (Ortiz-Karpf et al. 2016); the characteristics of the protolith are therefore unknown. The widespread erosion at the base of C1 suggests that a large volume of sediment was entrained, likely increasing the volume of the flow and modifying its rheology and dynamic behavior. Although the presence of several source areas may have contributed to the observed heterogeneity, this heterogeneity is thought to have been augmented by the entrainment of material from at least six, strongly heterogeneous, underlying units, comprising mainly channel-levee-complex sets (Fig. 5). The different degrees of disaggregation interpreted from the seismic facies can therefore reflect i) the different properties of the entrained units, ii) the different transport distances and strain histories experienced by sediment entrained at different points and times, and iii) the distribution of stress and strain in the flow. Despite this complicated interplay, the distribution of the seismic facies in C1 seems to correlate with the underlying bathymetry, with contraction updip of bathymetric highs, evidence of bypass above higher-gradient slopes, and increased disaggregation at the margins. This suggests that bathymetry was an important control on the internal characteristics of the deposit.

CONCLUSIONS

This paper uses 3D seismic reflection data from the Magdalena Fan, offshore Colombia, to show how mass-flow propagation across a bathymetrically complex slope and lithologically heterogeneous substrate influenced flow behavior and routing, and the geometry and internal characteristics of the associated MTCs. In particular:

i) Tectonic structures, which in this setting are represented by folds and thrusts, were the primary control on flow pathways and on the internal characteristics of MTC C1. Downdip of these structures, depositional relief, associated with channel-levee-complex sets, was a secondary control that, in some cases, influenced routing and process evolution, and therefore the internal characteristics of the MTCs.

ii) The axial orientations of channel-levee-complex sets with respect to MTC flow directions, together with the difference in levee height and mass flow thickness, determine whether mass flows are blocked, deflected, or confined by underlying channel levee complex sets. The style of interaction between mass flows and channel-levee-complex sets can influence mass-transport flow pathways, determine the type of substrate over which mass flows propagate, and influence flow-process evolution, runout distances, and the characteristics of the resulting deposits.

iii) The geometries of MTC basal surfaces were influenced by the nature of the underlying stratigraphic units, which are composed mainly of channel-levee-complex sets of different ages. Deeper erosion is observed above channel axes, which suggests preferential erosion of channel-fill deposits compared to adjacent external levee deposits. Also, more subtle variations in the morphology of the basal erosion surfaces occur above different levee units. These variations in the morphology of MTC erosion surfaces are interpreted to reflect compositional variability of the substrate, resulting in variable susceptibilities to erosion.

iv) Widespread erosion at the base of MTC C1 resulted in the entrainment of at least six underlying units, composed of channel-levee complexes and older MTCs. MTC heterogeneity, evidenced by different degrees of disaggregation and internal deformation, reflects the range of lithologies carried, the variable transport distances experienced by material entrained at different points and times, and the distribution of stress in the flow.

v) Seabed morphology was an important control on the distribution of intra-MTC seismic facies. Thus MTC C1 displays contraction updip of bathymetric highs, a predominance of

erosion and bypass above higher-gradient slopes, and increased disaggregation towards the margins. Further work is needed to establish whether such associations are generic.

ACKNOWLEDGEMENTS

The authors would like to thank Shell, Ecopetrol S.A. and Petrobras for supplying the data used for this study and Colciencias for providing the funding for the first author. We would also like to thank Lorena Moscardelli, Glenn Sharman, Andrea Fildani, and Gary Hampson for their constructive comments that helped improve this paper.

REFERENCES

Alfaro, E., and Holz, M., 2014, Seismic geomorphological analysis of deepwater gravity-driven deposits on a slope system of the southern Colombian Caribbean margin: *Marine and Petroleum Geology*, v. 57, p. 294-311.

Alves, T.M., 2010, 3D Seismic examples of differential compaction in mass-transport deposits and their effect on post-failure strata: *Marine Geology*, v. 271, p. 212-224.

Alves, T.M., 2015, Submarine slide blocks and associated soft-sediment deformation in deep-water basins: A review: *Marine and Petroleum Geology*, v. 67, p. 262-285.

Alves, T.M., and Cartwright, J.A., 2009, Volume balance of a submarine landslide in the Espírito Santo Basin, offshore Brazil: quantifying seafloor erosion, sediment accumulation and depletion: *Earth and Planetary Science Letters*, v. 288, p. 572-580.

Alves, T.M., Kurtev, K., Moore, G.F., and Strasser, M., 2014, Assessing the internal character, reservoir potential, and seal competence of mass-transport deposits using seismic texture: A geophysical and petrophysical approach: *American Association of Petroleum Geologists, Bulletin*, v. 98, p. 793-824.

Babonneau, N., Savoye, B., Cremer, M., and Bez, M., 2010, Sedimentary architecture in meanders of a submarine channel: Detailed study of the present Congo turbidite channel (Zaiango Project): *Journal of Sedimentary Research*, v. 80, p. 852–866.

Bernal-Olaya, R., Sanchez, J., Mann, P., and Murphy, M., 2015, Along-strike crustal thickness variations of the subducting Caribbean Plate produces two distinctive styles of thrusting in the offshore South Caribbean Deformed Belt, Colombia, *in* Bartolini, C. and Mann, P., eds., *Petroleum Geology and Potential of the Colombian Caribbean Margin*, American Association of Petroleum Geologists, Memoir 108, p. 295-322.

Breen, N.A., 1989, Structural effect of Magdalena fan deposition on the northern Colombia convergent margin: *Geology*, v. 17, p. 34–37.

Bull, S., Cartwright, J., and Huuse, M., 2009, A review of kinematic indicators from mass-transport complexes using 3D seismic data: *Marine and Petroleum Geology*, v. 26, p. 1132–1151.

Butler, R.W.H., and Tavarnelli, E., 2006, The structure and kinematics of substrate entrainment into high-concentration sandy turbidites: a field example from the Gorgoglione ‘flysch’ of southern Italy: *Sedimentology*, v. 53, p. 655-670.

Cardona, S., Wood, L.J., Day-Stirrat, R., and Moscardelli, L., 2016, Fabric development and pore-throat reduction in a mass-transport deposit in the Jubilee gas field, eastern Gulf of Mexico: Consequences for the sealing capacity of MTDs, *in* Lamarche, G., Mountjoy, J., Bull, S., Hubble, T., Krastel, S., Lane, E., Micallef, A., Moscardelli, L., Mueller, C., Pecher, I. and Woelz, S., eds., *Submarine Mass Movements and Their Consequences, Advances in Natural and Technological Hazards Research*, 41, Springer International, Switzerland, p. 27-37.

Cediel, F., Shaw, R.P., and Cáceres, C., 2003, Tectonic assembly of the northern Andean block, *in* Bartolini, C., Buffler, R.T., and Blickwede, J., eds., *The Circum-Gulf of Mexico and the Caribbean: Hydrocarbon Habitats, Basin Formation and Plate Tectonics*, American Association of Petroleum Geologists, Memoir 79, p. 815–848.

Clark, I.R., and Cartwright, J.A., 2009, Interactions between submarine channel systems and deformation in deepwater fold belts: Examples from the Levant Basin, Eastern Mediterranean sea: *Marine and Petroleum Geology*, v. 26, p. 1465–1482.

Clark, I.R., and Cartwright, J.A., 2012, Interactions between coeval sedimentation and deformation from the Niger delta deepwater fold belt, *in* Prather, B.E., Deptuck, M.E., Mohrig, D., Van Hoorn B. and Wynn, R.B., eds., *Application of the Principles of Seismic Geomorphology to Continental Slope and Base-of-Slope Systems: Case Studies from Seafloor and Near-Seafloor Analogues: SEPM, Special Publication 99*, p. 243-267.

Day, S., Llanes, P., Silver, E., Hoffmann, G., Warb, S., and Driscoll, N., 2015, Submarine landslide deposits of the historical lateral collapse of Ritter Island, Papua New Guinea: *Marine and Petroleum Geology*, v. 67, p. 419-438.

Deptuck, M.E., Steffens, G.S., Barton, M., and Pirmez, C., 2003, Architecture and evolution of upper fan channel-belts on the Niger Delta slope and in the Arabian Sea: *Marine and Petroleum Geology*, v. 20, p. 649–676.

Deptuck, M.E., Sylvester, Z., Pirmez, C., and O'Byrne, C., 2007, Migration–aggradation history and 3-D seismic geomorphology of submarine channels in the Pleistocene Benin-major Canyon, western Niger Delta slope: *Marine and Petroleum Geology*, v. 24, p. 406-433.

Ducassou, E., Fournier, L., Sierro, F.J., Zarikian, C.A., Lofi, J., Flores, J.A., and Roque, C., 2015, Origin of the large Pliocene and Pleistocene debris flows on the Algarve margin: *Marine Geology*, v. 377, p. 58-76.

Dunlap, D.B., Wood, L.J., Weisenberger, C., and Jabour, H., 2010, Seismic geomorphology of offshore Morocco's east margin, Safi Haute Mer area: *American Association of Petroleum Geologists, Bulletin*, v. 94, p. 615–642, doi: 10.1306/10270909055.

Duque-Caro, H., 1979, Major structural elements and evolution of northwestern Colombia, *in* Watkins, J.S., Montadert, L., and Dickerson, P.W., eds., *Geological and Geophysical Investigations of Continental Margins: American Association of Petroleum Geologists, Memoir 29*, p. 329–351.

Duque-Caro, H., 1984, Structural style, diapirism, and accretionary episodes of the Sinú-San Jacinto terrane, southwestern Caribbean borderland, *in* Bonini, W.E, Hargraves, R.B., and Shagam, R., eds., *The Caribbean-South American Plate Boundary and Regional Tectonics: Geological Society of America, Memoir 162*, p. 303–316.

Dykstra, M., Garyfalou, K., Kertznus, V., Kneller, B., Milana, J.P., Molinaro, M., Szuman, M., and Thompson, P., 2011, Mass-transport deposits: Combining outcrop studies and seismic forward modelling to understand lithofacies distributions, deformation, and their seismic stratigraphic expression, *in*, Shipp, C., Weimer, P., and Posamentier, H., eds., *Mass Transport Deposits in Deepwater Settings: SEPM, Special Publication 96*, p. 293-310.

Eggenhuisen, J.T., McCaffrey, W.D., Haughton, P.D.W., Butler, R.W.H, and Moore, I., 2010, Reconstructing large-scale remobilisation of deep-water deposits and its impact on sand-body architecture from cored wells: The Lower Cretaceous Britannia Sandstone Formation, UK North Sea: *Marine and Petroleum Geology*, v. 27, p. 1595-1615.

Frey-Martinez, J., 2010, 3D Seismic interpretation of mass transport deposits: Implications for basin analysis and geohazard evaluation, *in* Mosher, D.C., Shipp, R.C., Moscardelli, L., Chaytor, J.D., Baxter, C.D.P., Lee, H.J., and Urgeles, R., eds., *Submarine Mass Movements and Their Consequences: Springer, Netherlands*, p. 553-568.

Frey-Martinez, J., Cartwright, J., and Hall, B., 2005, 3D seismic interpretation of slump complexes: examples from the continental margin of Israel: *Basin Research*, v. 17, p. 83–108.

Frey-Martinez, J., Cartwright, J., and James, D., 2006, Frontally confined versus frontally emergent submarine landslides: A 3D seismic characterisation: *Marine and Petroleum Geology*, v. 23, p. 585–604.

Gamboa, D., Alves, T., Cartwright, J., and Terrinha, P., 2010, MTD distribution on a 'passive' continental margin: the Espírito Santo Basin (SE Brazil) during the Palaeogene: *Marine and Petroleum Geology*, v. 27, p. 1311-1324.

Gamboa, D., Alves, T.M., and Cartwright, J., 2011, Distribution and characterization of failed (mega) blocks along salt ridges, southeast Brazil: Implications for vertical fluid flow on continental margins: *Journal of Geophysical Research*, v. 116, no. B08103.

Gee, M.J.R., Gawthorpe, R.L., and Friedmann, S.J., 2006, Triggering and evolution of a giant submarine landslide, offshore Angola, revealed by 3D seismic stratigraphy and geomorphology: *Journal of Sedimentary Research*, v. 76, p. 9-19.

Gee, M.J.R., Uy, H.S., Warren, J., Morley, C.K., and Lambiase, J. J., 2007, The Brunei slide: A giant submarine landslide on the North West Borneo Margin revealed by 3D seismic data: *Marine Geology*, v. 246, p. 9-23.

Georgiopoulou, A., Masson, D.G., Wynn, R., and Krastel, S., 2010, Sahara Slide: Age, initiation, and processes of a giant submarine slide: *Geochemistry, Geophysics, Geosystems*, v. 11, no. Q07014.

Hansen, L.A.S., Callow, R.H.T., Kane, I.A., Gamberi, F., Rovere, M., Cronin, B.T., and Kneller, B.C., 2015, Genesis and character of thin-bedded turbidites associated with submarine channels: *Marine and Petroleum Geology*, v. 67, p. 852–879.

Heiniö, P., and Davies, R.J., 2006, Degradation of compressional fold belts: deep-water Niger Delta: *American Association of Petroleum Geologists, Bulletin*, v. 90, p. 753–770.

Hodgson, D.M., Di Celma, C.N., Brunt, R.L., and Flint, S.S., 2011, Submarine slope degradation, aggradation and the stratigraphic evolution of channel–levee systems: *Geological Society of London, Journal [of the]*, v. 168, p. 625–628.

Hubbard, S.M., Covault, J.A., Fildani, A., and Romans, B.W., 2014, Sediment transfer and deposition in slope channels: deciphering the record of enigmatic deep-sea processes from outcrop: *Geological Society of America, Bulletin*, v. 126, p. 857–871.

Iverson, R., 1997, The physics of debris flows: *Reviews of Geophysics*, v. 35, p. 245-296.

Iverson, R., 2012, Elementary theory of bed-sediment entrainment by debris flows and avalanches: *Journal of Geophysical Research*, v. 117, no. F03006.

Jackson, C.A.-L., 2011, Three-dimensional seismic analysis of megaclast deformation within a mass transport deposit; implications for debris flow kinematics: *Geology*, v. 39, p. 203–206.

Jackson, C.A.-L., and Johnson, H., 2009, Sustained turbidity currents and their interaction with debris-related topography; Labuan Island, offshore NW Borneo, Malaysia: *Sedimentary Geology*, v. 219, p. 77-96.

Joanne, C., Lamarche, C., and Collot, J.-Y., 2013, Dynamics of giant mass transport in deep submarine environments: The Matakaoa Debris Flow, New Zealand: *Basin Research*, v. 25, p. 471-488.

Jobe, Z.R., Sylvester, Z., Parker, A.O., Howes, N.C., Slowey, N., and Pirmez, C., 2015, Rapid adjustment of submarine channel architecture to changes in sediment supply: *Journal of Sedimentary Research*, v. 85, p. 729–753.

Johnson, C.G., Kokelaar, B.P., Iverson, R., Logan, M., Lahusen, R.G., and Gray, J.M.N.T., 2012, Grain-size segregation and levee formation in geophysical mass flows: *Journal of Geophysical Research, Earth Surface*, v. 117, no. F01032.

Jones, G., Mayall, M., and Lonergan, L., 2012, Contrasting depositional styles on a slope system and their control by salt tectonics: through-going channels, ponded fans, and mass transport complexes, *in* *New Understanding of the Petroleum Systems of Continental Margins of the World: Gulf Coast Section 032, SEPM*, p. 503 – 533.

Kane, I.A., and Hodgson, D.M., 2011, Sedimentological criteria to differentiate submarine channel levee subenvironments: Exhumed examples from the Rosario Fm. (Upper Cretaceous) of Baja California, Mexico, and the Fort Brown Fm. (Permian), Karoo Basin, S. Africa: *Marine and Petroleum Geology*, v. 28, p. 807–823.

Kneller, B., Dykstra, M., Fairwather, L., and Milana, P., 2015, Mass-transport and slope accommodation: Implications for turbidite sandstone reservoirs: *American Association of Petroleum Geologists, Bulletin*, v. 100, p. 213-235.

Kolla, V., and Buffler, R.T., 1984, Morphologic, acoustic, and sedimentologic characteristics of the Magdalena Fan: *Geo-Marine Letters*, v. 3, p. 85-91.

Lamarche, G., Joanne, C., and Collot, J.Y., 2008, Successive, large mass-transport deposits in the south Kermadec fore-arc basin, New Zealand: The Matakaoa Submarine Instability Complex: *Geochemistry, Geophysics, Geosystems*, v. 9, no. Q04001.

Lee, C., Nott, J.A., and Keller, F.B., 2004, Seismic expression of the Cenozoic mass transport complexes, deepwater Tarfaya–Agadir Basin, Offshore Morocco: Offshore Technology Conference, 3 May–6 May 2004, Houston, Texas, 16741-MS, 18 p., doi: 10.4043/16741-MS.

Locat, J., and Lee, H., 2005, Subaqueous debris flows, *in* Jakob, M., and Hungr, O., eds., *Debris-flow Hazards and Related Phenomena*: Springer, Berlin, p. 203-245.

Major, J.T., 1997, Processes in large-scale debris-flow experiments: *The Journal of Geology*, v. 105, p. 345-366.

Martinez, J., Castillo, J., Ortiz-Karpf, A., Rendon, L., Mosquera, J.C., and Vega, V., 2015, Deep water untested oil-play in the Magdalena Fan, Caribbean, Colombian Basin, *in* Bartolini, C., and Mann, P., eds., *Petroleum Geology and Potential of the Colombian Caribbean Margin*: American Association of Petroleum Geologists, Memoir 108, p. 251-260.

Mayall, M., Jones, E., and Casey, M., 2006, Turbidite channel reservoirs: Key elements in facies prediction and effective development: *Marine and Petroleum Geology*, v. 23, p. 821-841.

McGilvery, T.A., Haddad, G., and Cook, D.L., 2004, Seafloor and shallow subsurface examples of mass transport complexes, offshore Brunei, *in* Offshore Technology Conference, Proceedings, Paper 16780.

Meckel, L.D. III, 2011, Reservoir characteristics and classification of sand-prone submarine mass-transport deposits, *in* Shipp, C., Weimer, P., and Posamentier, H., eds., *Mass-transport deposits in deepwater settings*, SEPM, Special Publication, v. 96, p. 423–450.

Meckel, L.D. III, Angelatos, M., Bonnie, J., McGarva, R., Almond, T., Marshall, N., Bourdon, L., and Aurisch, K., 2011, Reservoir characterization of sand-prone mass-transport deposits within slope canyons, *in* Shipp, C., Weimer, P., and Posamentier, H., eds., *Mass-Transport Deposits in Deepwater Settings*, SEPM, Special Publication 96, p. 391-421.

Mehta, A.J., McAnally, W.H. Jr., Hayter, E.J., Teeter, A.M., Schoellhamer, D., Heltzel, S.B., and Carey, W.P., 1989, Cohesive sediment transport. II: Application: *Journal of Hydraulic Engineering*, v. 115, p. 1094-1112.

Meschede, M., and Frisch, W., 1998, A plate-tectonic model for the Mesozoic and early Cenozoic history of the Caribbean plate: *Tectonophysics*, v. 296, p. 269–291.

Migeon, S., Savoye, B., Zanella, E., Mulder, T., Faugères, J.-C., and Weber, O., 2001, Detailed seismic-reflection and sedimentary study of turbidite sediment waves on the Var

Sedimentary Ridge (SE France): Significance for sediment transport and deposition and for the mechanisms of sediment-wave construction: *Marine and Petroleum Geology*, v. 18, p. 179-208.

Morris, E.A., Hodgson, D.M., Brunt, R.L., and Flint, S.S., 2014, Origin, evolution and anatomy of silt-prone submarine external levees: *Sedimentology*, v. 61, p. 1734–1763.

Moscardelli, L., Wood, L., and Mann, P., 2006, Mass-transport complexes and associated processes in the offshore area of Trinidad and Venezuela: *American Association of Petroleum Geologists, Bulletin*, v. 90, p. 1059–1088.

Nakajima, T., Satoh, M., and Okamura, Y., 1998, Channel-levee complexes, terminal deep-sea fan and sediment wave fields associated with the Toyama Deep-Sea Channel system in the Japan Sea: *Marine Geology*, v. 147, p. 25-41.

Nakajima, T., and Kneller, B.C., 2013, Quantitative analysis of the geometry of submarine external levees: *Sedimentology*, v. 60, p. 877–910.

Olafiranye, K., Jackson, C.A.-L., and Hodgson, D.M., 2013, The role of tectonics and mass-transport complex emplacement on upper slope stratigraphic evolution: A 3D seismic case study from offshore Angola: *Marine and Petroleum Geology*, v. 44, p. 196–216.

Omosanya, K.O., and Alves, T.M., 2013, A 3-dimensional seismic method to assess the provenance of mass-transport deposits (MTDs) on salt-rich continental slopes (Espírito Santo Basin, SE Brazil): *Marine and Petroleum Geology*, v. 44, p. 223-239.

Ortiz-Karpf, A., Hodgson, D.M., and McCaffrey, W.D., 2015, The role of mass-transport complexes in controlling channel avulsion and the subsequent sediment dispersal patterns on an active margin: The Magdalena Fan, offshore Colombia: *Marine and Petroleum Geology*, v. 64, p. 58-75.

Ortiz-Karpf, A., Hodgson, D.M., Jackson, C.A.-L., and McCaffrey, W.D., 2016, Mass-transport complexes as markers of deep-water fold-and-thrust belt evolution: Insights from the southern Magdalena Fan, offshore Colombia: *Basin Research*, doi:10.1111/bre.12208.

Pindell, J.L., 1994, Evolution of the Gulf of Mexico and the Caribbean, *in* Donovan, S.K., and Jackson, T.A., eds., *Caribbean Geology. An Introduction*, University of the West Indies Publisher's Association, p. 13–39.

Pindell, J.L., and Kennan, L., 2009, Tectonic evolution of the Gulf of Mexico, Caribbean and northern South America in the mantle reference frame: An update, *in* James, K.H., Lorente,

M.A., and Pindell, J.L., eds., *The Origin and Evolution of the Caribbean Plate*: Geological Society of London, Special Publication, 328, p. 1–55.

Piper, D.J.W., and Normark, W.R., 2001, Sandy fans—from Amazon to Hueneme and beyond: *American Association of Petroleum Geologists, Bulletin*, v. 85, p. 1407-1438.

Pirmez, C., Hiscott, R.N., and Kronen, J.D., 1997, Sandy turbidite successions at the base of channel-levee systems of the Amazon Fan revealed by FMS logs and cores: Unravelling the facies architecture of large submarine fans, *in Proceedings of the Ocean Drilling Program. Scientific results*, 155, 7–33.

Posamentier, H.W., and Kolla, V., 2003, Seismic geomorphology and stratigraphy of depositional elements in deep-water settings: *Journal of Sedimentary Research*, v. 73, p. 367–388.

Posamentier, H.W., and Martinsen, O.J., 2011, The character and genesis of submarine mass-transport deposits: insights from outcrop and 3D seismic data, *in Shipp, C., Weimer, P., and Posamentier, H., eds., Mass-Transport Deposits in Deepwater Settings*: SEPM, Special Publication 96, p. 7–38.

Prior, D.B., Bornhold, B.D., and Johns, M.W., 1984, Depositional characteristics of submarine debris flow: *The Journal of Geology*, v.92, p. 707-727.

Romero-Otero, G.A., 2009, Deepwater sedimentary processes in an active margin, Magdalena submarine fan, offshore Colombia: PhD Thesis, University of Oklahoma, 298p.

Romero-Otero, G.A., Slatt, R.M., and Pirmez, C., 2010, Detached and shelf-attached mass transport complexes on the Magdalena deepwater fan, *in Mosher, D.C., Shipp, R.C., Moscardelli, L., Chaytor, J.D., Baxter, C.D.P., Lee, H.J., and Urgeles, R., eds., Submarine Mass Movements and Their Consequences*: Springer, Netherlands, p. 153-166.

Shanmugam, G., Lehtonen, L.R., Straume, T., Syvertsen, S.E., Hodgkinson, R.J., and SKIBELI, M., 1994, Slump and debris-flow dominated upper slope facies in the Cretaceous of the Norwegian and Northern North Seas (61–67°N): Implications for sand distribution: *American Association of Petroleum Geologists, Bulletin*, v. 78, p. 910-937.

Skene, K., Piper, D.J.W., and Hill, P.A., 2002, Quantitative analysis of variations in depositional sequence thickness from submarine channel levees: *Sedimentology*, v. 49, p. 1411-1430.

Sobiesiak, M., Kneller, B., Alsop, I.G., and Milana, J.P., 2016, Internal deformation and kinematic indicators within a tripartite mass transport deposit, NW Argentina: *Sedimentary Geology*, v. 344, p. 364-381.

Steffens, G.S., Biegert, E.K., Sumner, H.S, and Bird, D., 2003, Quantitative bathymetric analyses of selected deepwater siliciclastic margins: receiving basin configurations for deepwater fan systems: *Marine and Petroleum Geology*, v. 20, p. 547-561.

Stevenson, C.J., Jackson, C.A.L., Hodgson, D.M., Hubbard, S.M., and Eggenhuisen, J.T., 2015, Deep-water sediment bypass: *Journal of Sedimentary Research*, v. 85, p. 1058-1081.

Stow, D.A.V., Reading, H.G., and Collinson, J.D., 1996, Deep seas, *in* Reading, H.G., ed., *Sedimentary Environments*, Third Edition: Oxford, Blackwell Science, p. 395-454.

Strachan, L., 2008, Flow transformations in slumps: a case study from the Waitemata Basin, New Zealand: *Sedimentology*, v. 55, p. 1311-1332.

Vinnels, J.S., Butler, R.W.H., McCaffrey, W.D., and Paton, D.A., 2010, Depositional processes across the Sinú accretionary prism, offshore Colombia: *Marine and Petroleum Geology*, v.27, p. 794–809.

Weimer, P., and Shipp, C., 2004, Mass transport complex: Musing on past uses and suggestions for future directions, *in* *Offshore Technology Conference, Proceedings*, Paper 16752.

Weimer, P., and Slatt, R.M., 2007, Deepwater reservoir elements: Mass-transport deposits and slides, *in* *Introduction to the Petroleum Geology of Deepwater settings*, American Association of Petroleum Geologists, *Studies in Geology*, v. 57, p. 9-419.

Zeng, H., Henry, S.C., Riola, J.P., 1998, Stratal slicing, part II: Real 3-D seismic data: *Geophysics*, v. 63, p. 514-522.

Figure 1. Geological setting. **A)** The Magdalena Fan is located in an active margin where the Caribbean Plate collides obliquely with the South American Plate. **B)** The Magdalena Fan is located in a relatively undeformed area between the Southern Sinú Fold Belt (SSFB) and the Northern Sinú Fold Belt (NSFB). The study area, defined by the black rectangle includes the northern part of the SSFB and part of the relatively undeformed area.

Figure 2. Structural elements. **A)** Seabed dip map colored by subsurface elevation. To the SE of the study area, two thrust sheets develop, the Updip Anticline and the Downdip Anticline. The northern part of the Downdip Anticline is not expressed on the seabed and its axis is projected from the subsurface. The rest of the study area is dominated by channel-levee-complex sets. **B)** Depth slice combining variance and amplitude, see parts C-E for intersection. The Downdip Anticline is subdivided in two segments separated by a saddle, the southern Downdip Anticline and the northern Downdip Anticline. The Downdip Anticline is separated from the Updip Anticline by a syncline. **C)** The northern Downdip Anticline is not faulted and is more symmetric. **D)** The southern Downdip Anticline is faulted and asymmetric. **E)** The northern Downdip Anticline and the southern Downdip Anticline are separated by a saddle. Several MTCs developed on these structures.

Figure 3. Location of the MTCs in the study area. **A)** Variance extraction colored by subsurface elevation at the composite surface defined as Unit D by Ortiz-Karpf et al. (2015) showing the areal extent of the MTCs in the study area. The colored polygons represent the

outline of the MTCs. **B)** Seismic section across the MTCs showing their temporal and spatial relationships. MTCs S1-S3 onlap the southern levee of Unit I, while S4 overlies Unit I and is mostly concentrated to the NW of its northern levee. Unit IV also constitutes the northwestern limit of S5 and S6 and the southeastern limit of C1.

Figure 4. Seismic units underlying the MTCs. **A)** Geoseismic cross section based on the seismic line in Figure 3B showing the relationship between the MTCs and the channel-levee-complex sets. **B)** Schematic section showing the inferred configuration of the channel-levee-complex sets in units I to VI prior to the emplacement of the MTCs.

Figure 5. Substrate Map. **A)** Map showing the configuration of the substrate directly underlying the MTCs. Unit I is the oldest and VI is the youngest. All of them are composed of channel-levee-complex sets. The brown polygons represent older MTCs. The black lines show the location of the cross sections in Figures 6 and 10. **B)** Substrate maps overlain with the polygons defining the outline of the overlying MTCs. The black line indicates the location of Figure 3B. **C)** General trend of the channel axes of units I-VI. Note that the axes of units IV and VI are almost entirely eroded and the axis of Unit V is absent outboard of the northern Downdip Anticline.

Figure 6. Seismic cross sections showing the morphology of the basal surfaces and the configuration of the substrate. See Figure 5 for location. **A)** MTC C1 is bounded to the NW by Unit III and to the SE by Unit IV. Unit IV is also eroded by MTCs S4-S6. MTCs S1-S3 onlap the levee of Unit I. **B)** Unit III separates N1 and N2 from C1. To the SE C1 overlies units I and IV. Note the high-amplitude discontinuous reflections in Unit D, which are interrupted as remnants of its channel axis. **C)** N1 and N2 are bounded by units II, III, V, and VI. The channel axes of units V and VI have been completely removed, and there is a deeply incised MTC underlying N1. Towards the east, the basal surface of C1 is steeper across Units V and VI and flattens on Unit II. **D)** To the NE, the composite basal surface of N1 and N2 incises more deeply above the channel axis of Unit V. The axis of Unit VI was completely

eroded. Unit VI is affected by faults that dip into the MTC erosion surfaces. The slope of the basal surface of C1 is steeper above Unit V than above Unit II.

Figure 7. Bounding surfaces of C1. **A)** Variance extraction colored by subsurface elevation showing the basal surface of C1 and the composite basal surface of N1 and N2. Note the trajectory of C1 and its relationship to the anticlines and the erosional trough that connects the erosional fairway of C1 with that of N1 and N2. **B)** Variance extraction colored by subsurface elevation at the top of MTC C1. The irregularities are related to underlying megaclasts. **C)** Cross section across the erosional cut across the northern Downdip Anticline connecting C1 to N1 and N2. The location of the cut possibly coincides with the location of the eroded channel axis of Unit VI. **D)** Section along the erosional cut between C1 and N1 and N2 showing an MTC remnant overlying the erosion surface.

Figure 8. Downdip changes in the morphology of C1. **A)** Perspective view of the basal surface of C1 showing the location of the sections shown in parts C-G. **B)** View between the northern Downdip Anticline and the Updip Anticline showing that C1 followed the orientation of the syncline. **C-G)** Seismic cross sections showing that the height and slope of the lateral walls of C1 decreases downdip and highlighting changes in the slope of the lateral margins which are sometimes related to changes in the substrate units.

Figure 9. Thickness, variance, and facies maps of C1. **A)** Vertical thickness map of C1. **B)** Variance extraction at the interval between 50-75% of the vertical thickness of C1 from base to top. Note the character of the seismic facies, with facies 1 having the lowest variance, facies 3 having the highest variance and facies 2 having an intermediate variance. **C)** Variance extraction of the top quarter of C1 showing the appearance of the megaclasts. **D)** Seismic facies map of C1.

Figure 10. Uninterpreted and interpreted sections along the center of MTC C1 showing the down-dip distribution of the seismic facies. See figures 5A and 9 for location.

Figure 11. Seismic cross sections showing the examples of the seismic facies in C1, see Figure 9 for location. **A.** Uninterpreted and interpreted sections across the downdip anticline. Note the change in thickness and megaclast abundance above the crest of the anticline. **B)** Uninterpreted and interpreted sections across C1 towards the downdip limit of the dataset. Note the erosion at the base and the presence of large megaclasts.

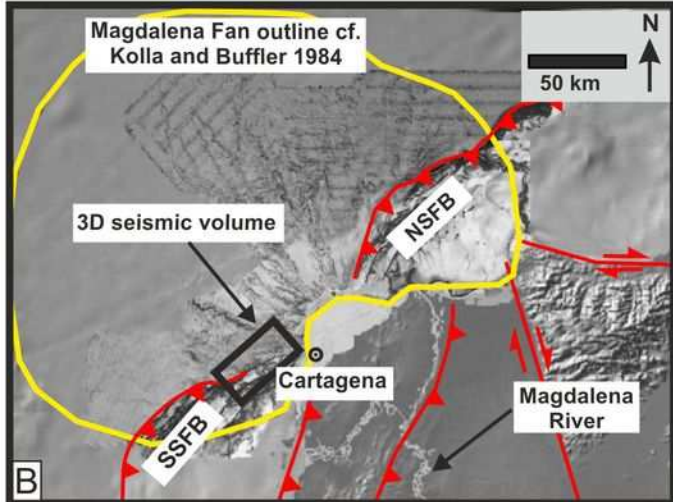
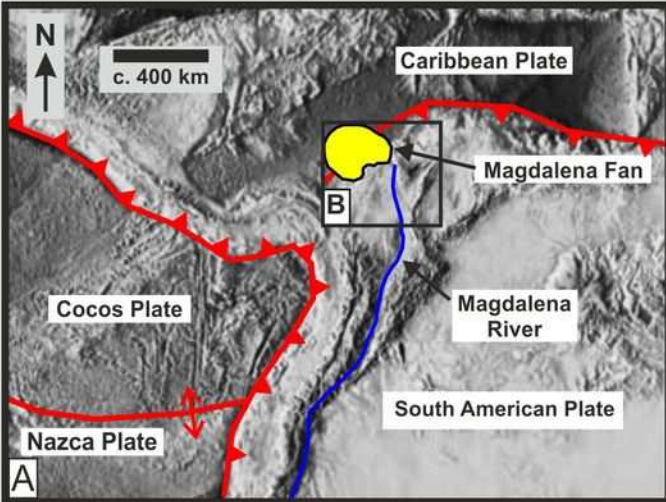
Figure 12. Dimensions and distribution of the megaclasts in C1. **A)** Pie chart showing the percentage of megaclasts found in various regions of MTC C1. **B)** Relationship between the length of the short and long axes of the megaclasts. Measurements are taken from map-view geometries. **C)** Relationship between the vertical thickness of the megaclasts and the length of the long axes.

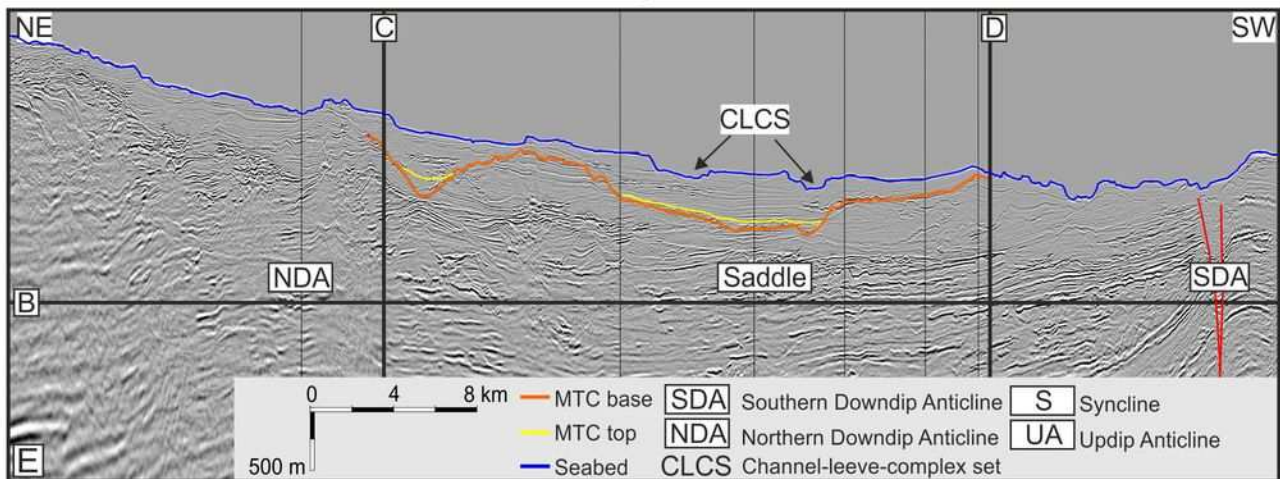
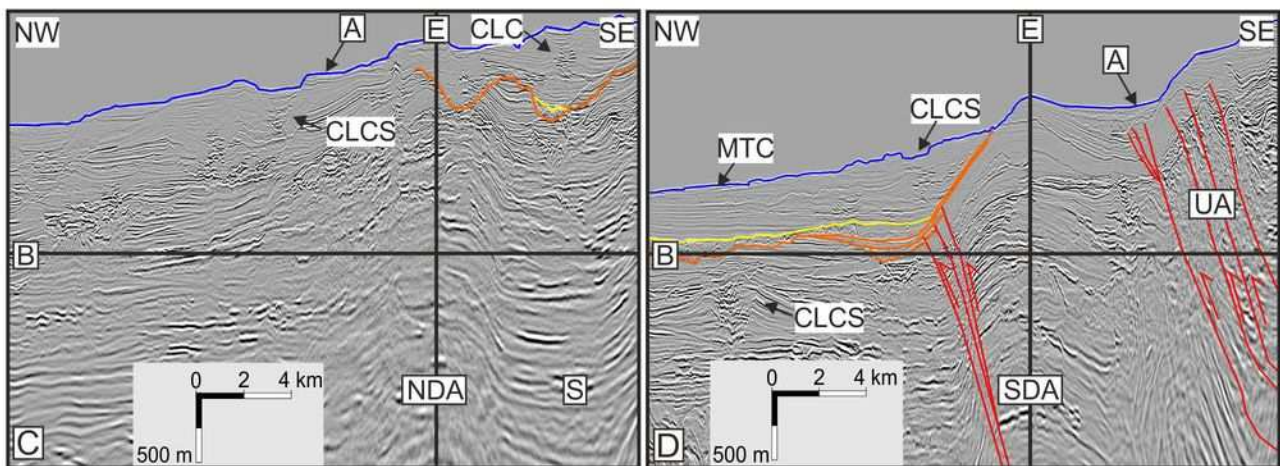
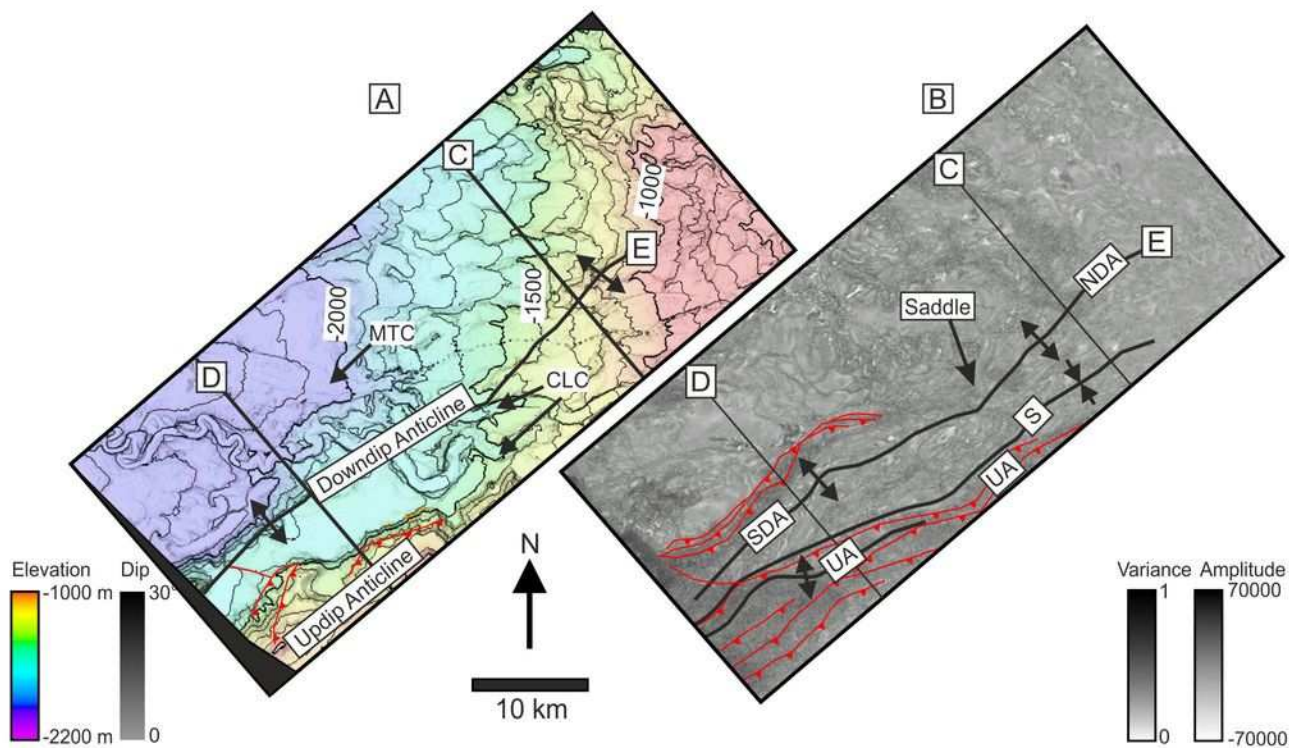
Figure 13. Grooves at the base of C1. **A)** Variance extraction at the base of C1 showing the presence of lineaments parallel to the lateral scarps which are interpreted as grooves. Also note the presence of lateral scarps in the margins, which are interpreted as areas of local collapse. **B)** Seismic cross section across the grooves, showing their V-shaped morphology.

Figure 14. Simplified cartoon representation of the main bathymetric and substrate controls on MTCs and the types of interactions between MTCs and channel-levee-complex sets. From left to right: Type 1: An MTC exploiting an underlying channel-levee-complex set has incised deeply above the channel axis and widens the erosion surface by eroding the external levees less deeply. Type 2: An MTC focused along an interchannel low. Type 3: An MTC is deflected by the levee of a channel-levee-complex. Type 4: An MTC is blocked by a highly oblique channel-levee-complex set. Note that contractional seismic facies develop updip of bathymetric highs, and erosion and bypass dominate areas of steeper axial gradients.

Figure 15. Distribution of the megaclasts with respect to the grooves on the basal surface of C1. The presence of grooves indicates that some megaclasts were transported for several kilometers, possibly across the Downdip Anticline. On the southern downdip margin of C1

some megaclasts are clustered above erosional scours, suggesting local erosion. Arcuate scarps on the flanks of syncline may also have been sources of megaclasts.





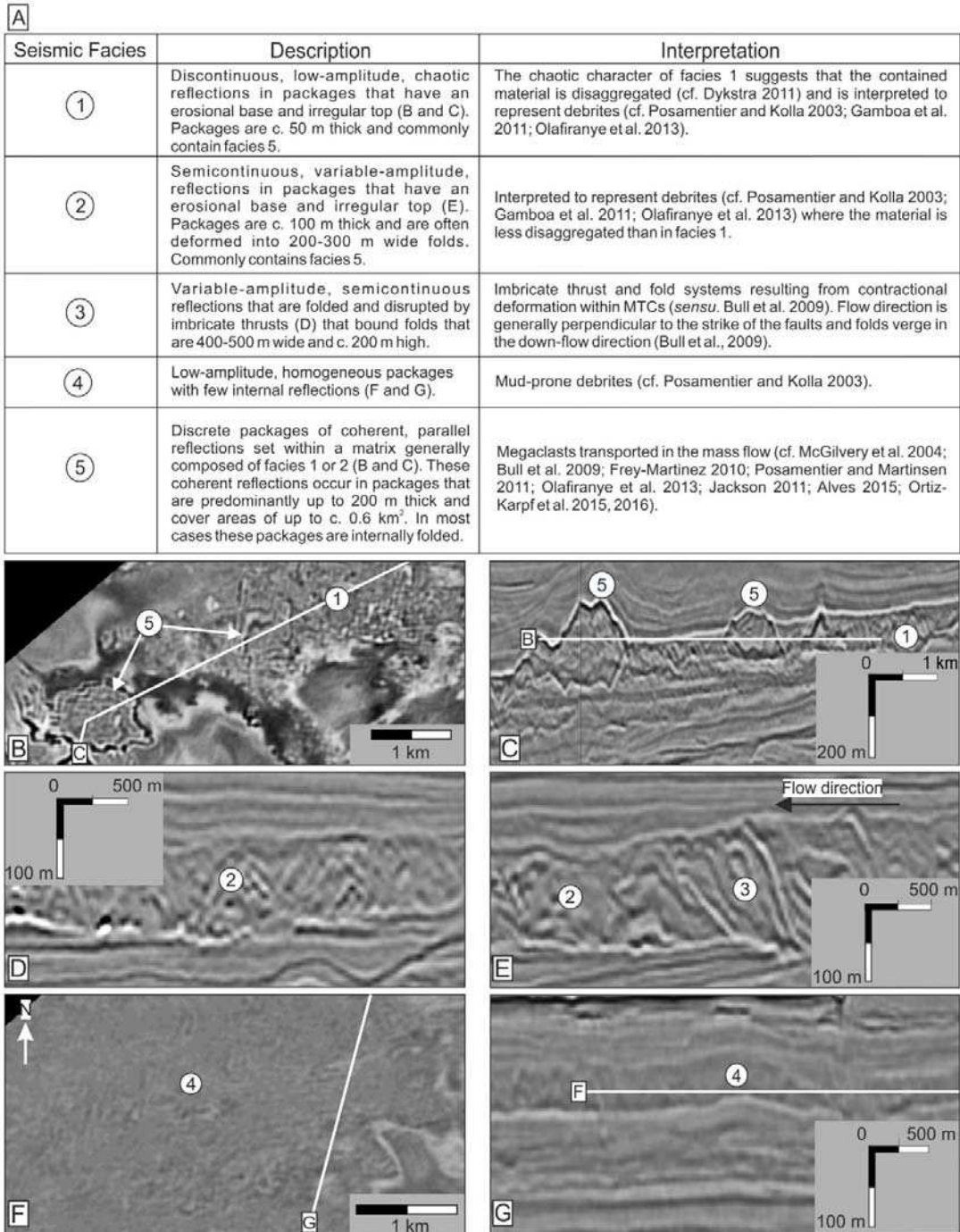
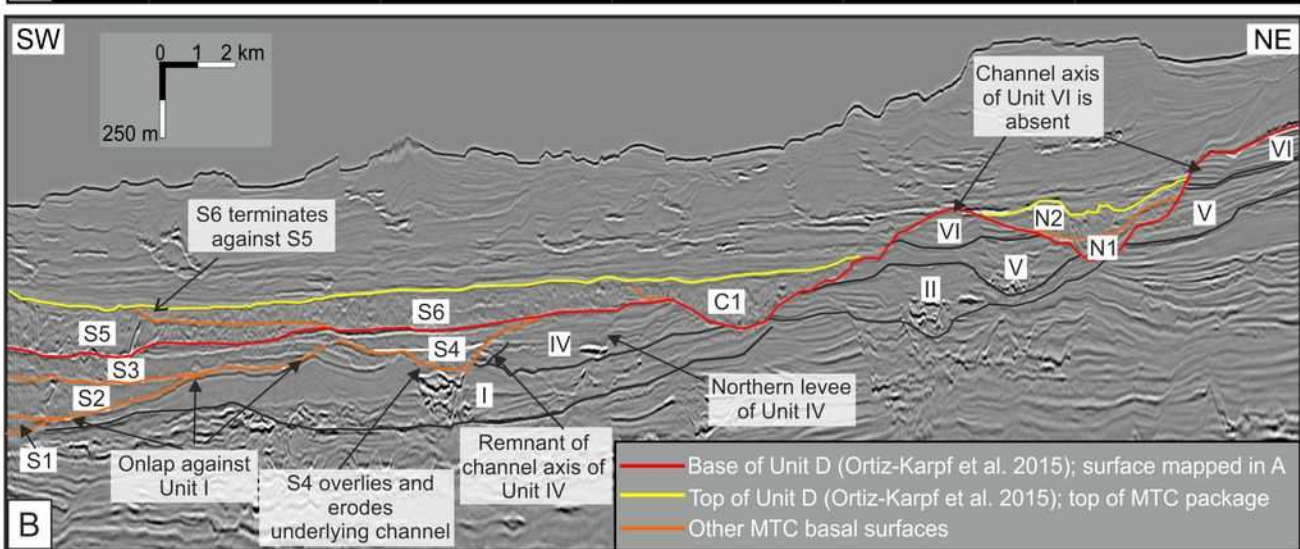
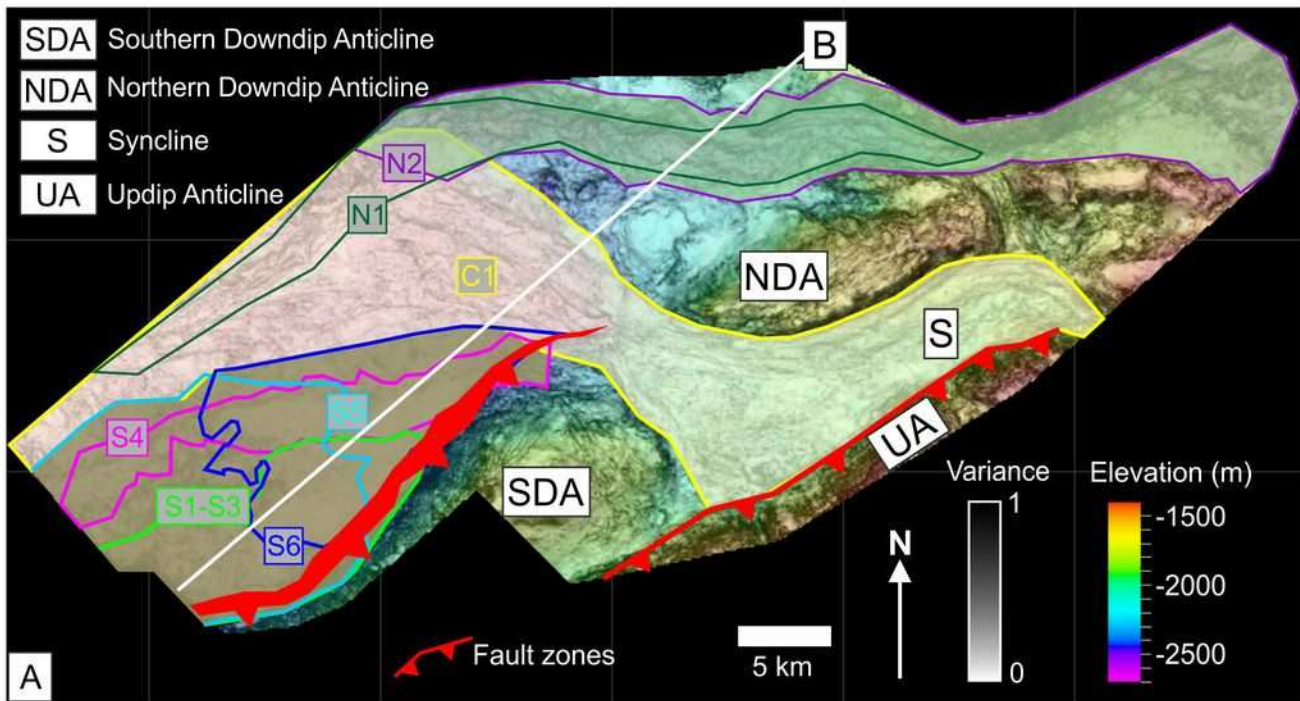
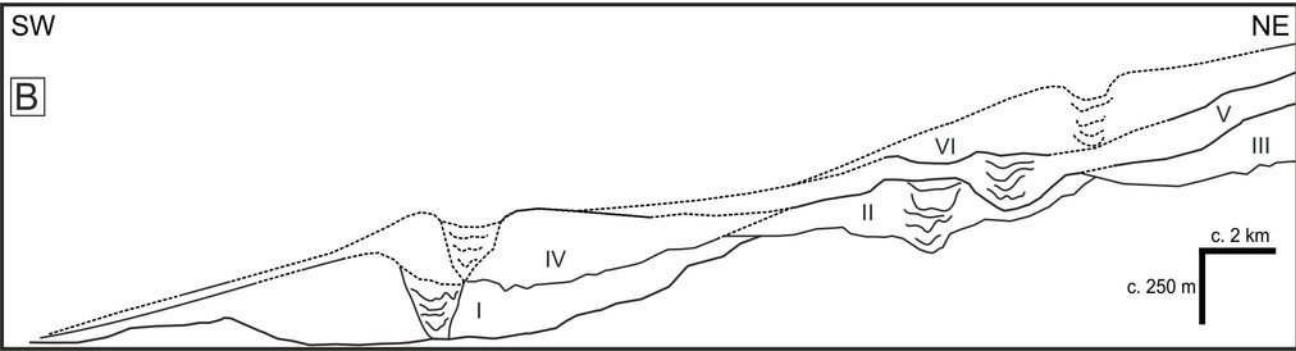
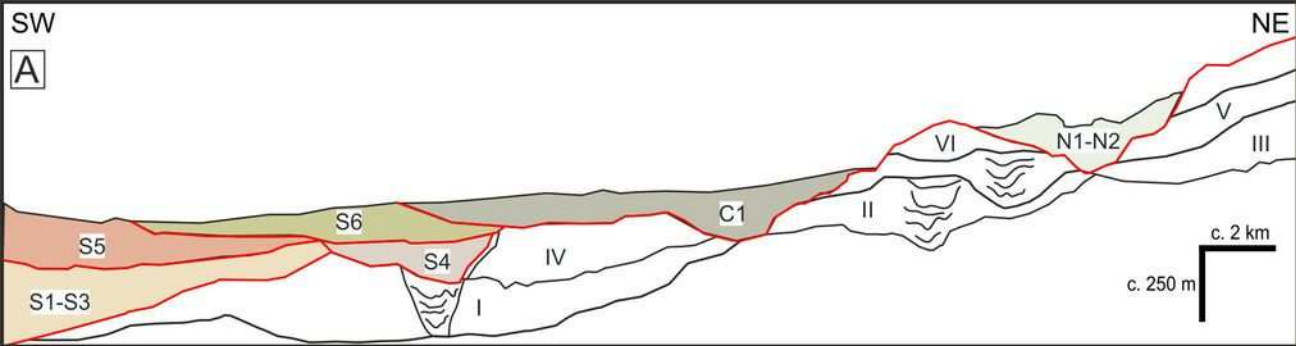
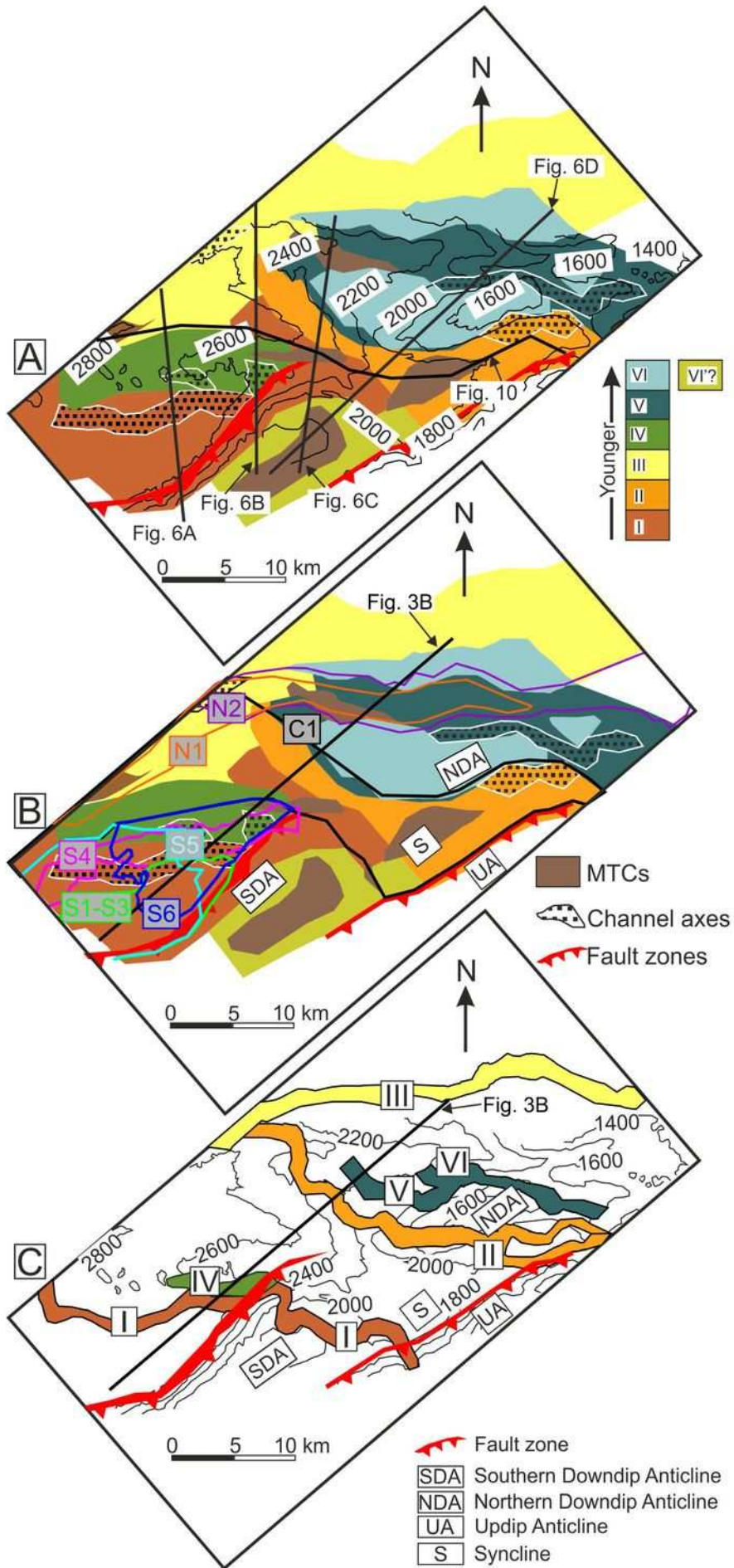


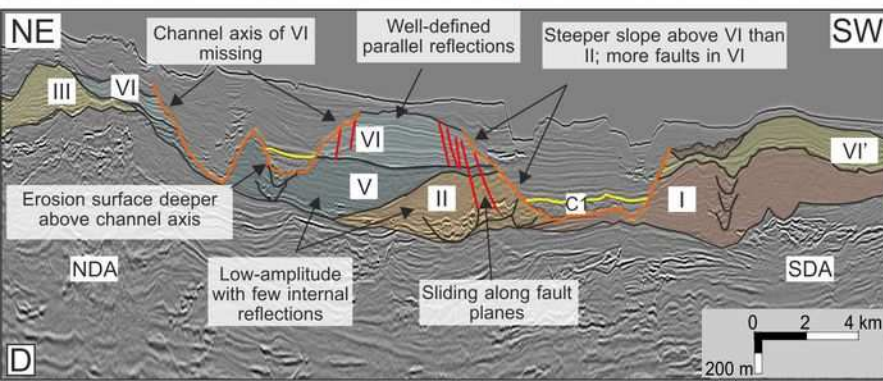
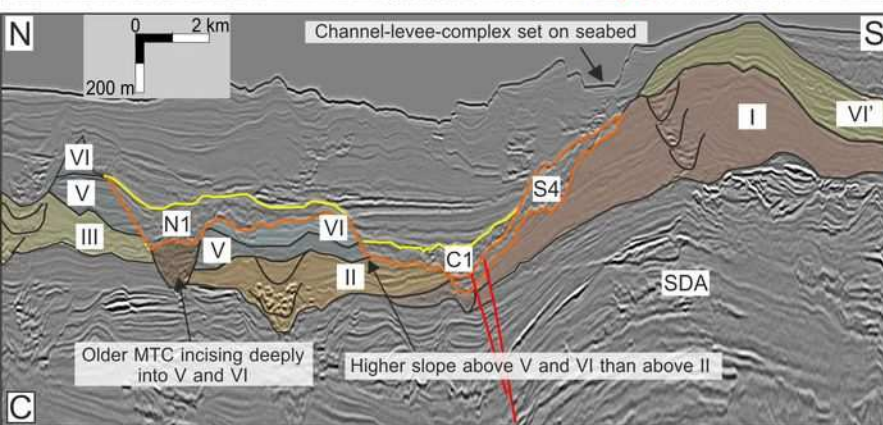
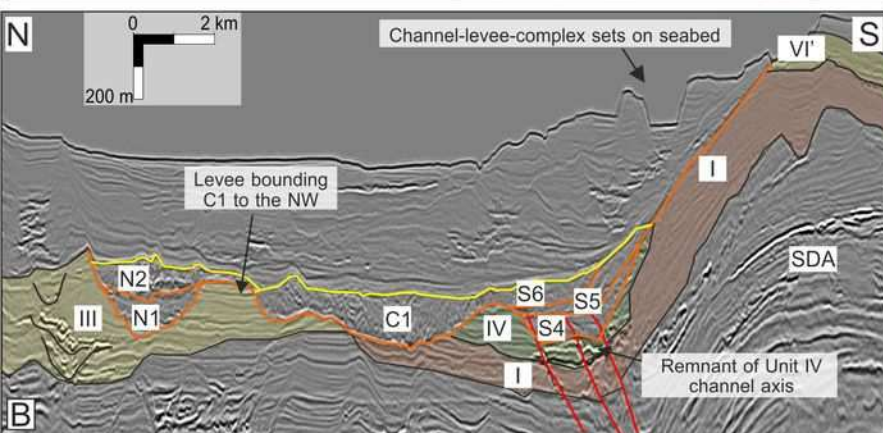
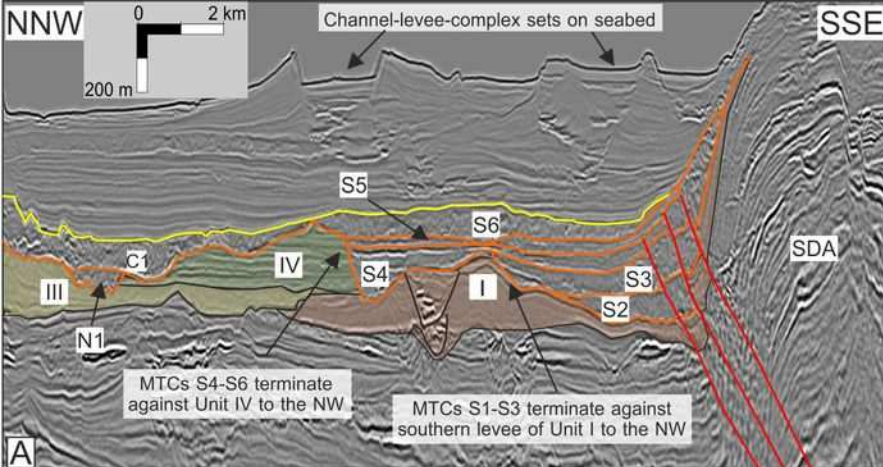
Table 1. MTC seismic-facies classification. **A)** Description and interpretation of the seismic facies. **B)** Depth slice showing the map-view appearance of facies 5 and 1 (see C for intersection). **C)** Cross section across A showing facies 1 and 5. **D)** Seismic cross section showing the appearance of facies 2. Note the semicontinuous folded reflections. **E)** Seismic

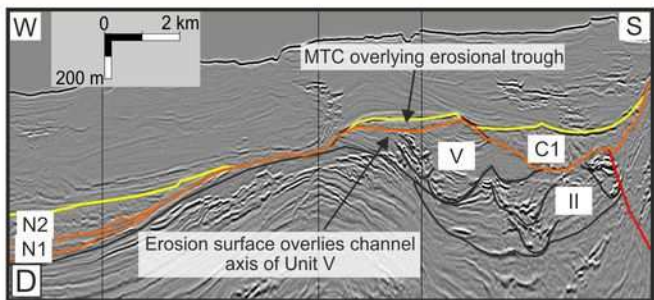
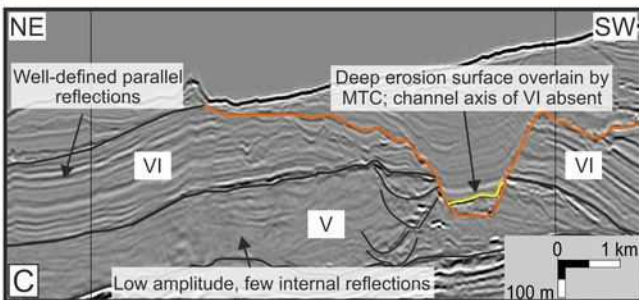
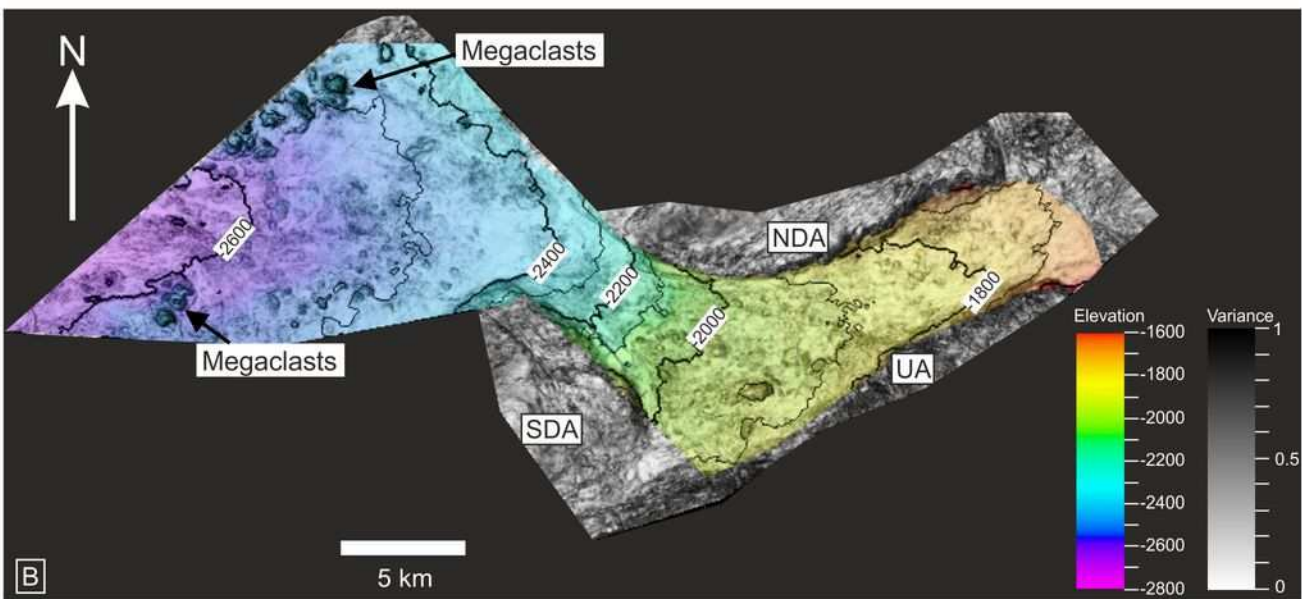
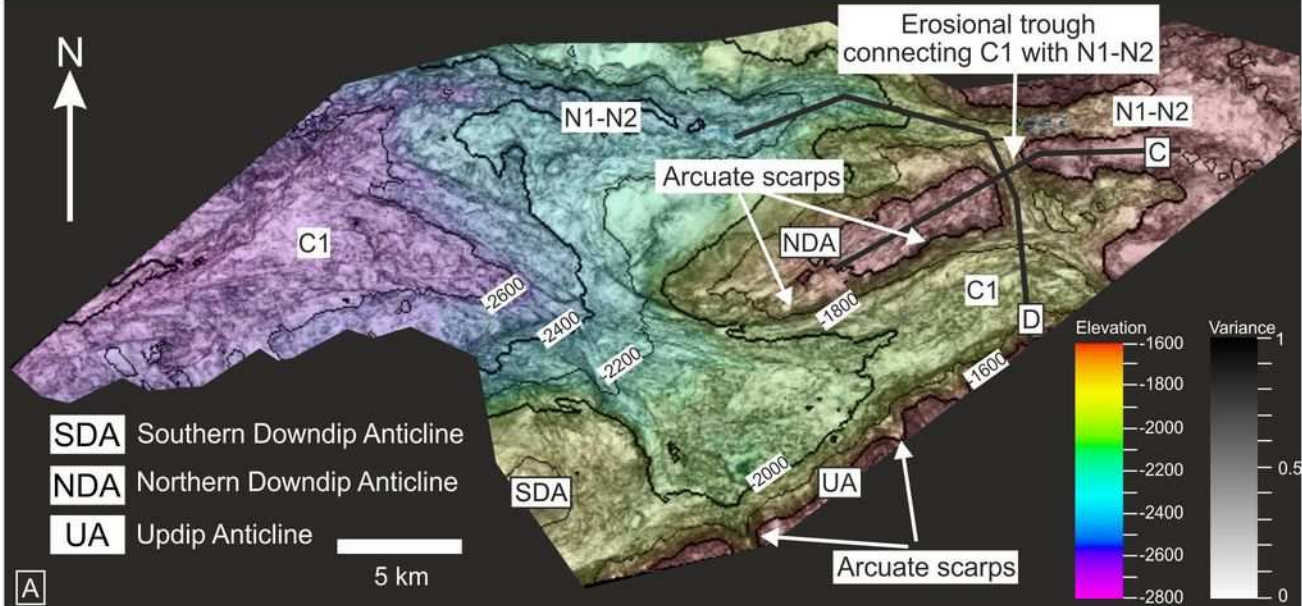
cross section showing imbricate thrust systems in facies 3. **F)** Depth slice showing the appearance of facies 4, see G for intersection. **G)** Cross section showing facies 4. Note the low-amplitude, homogeneous character.

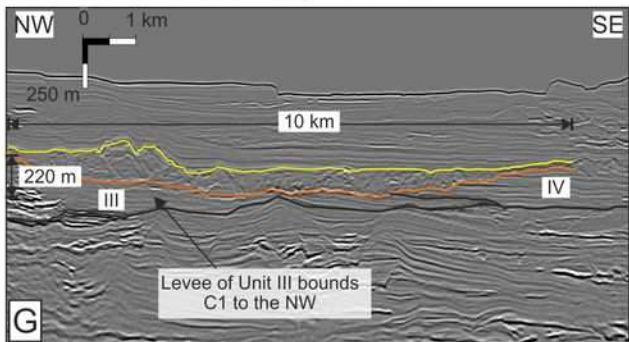
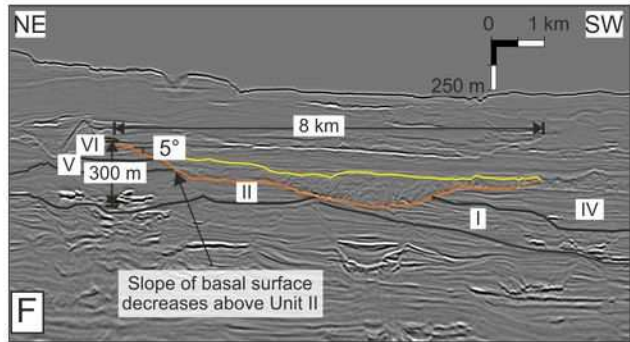
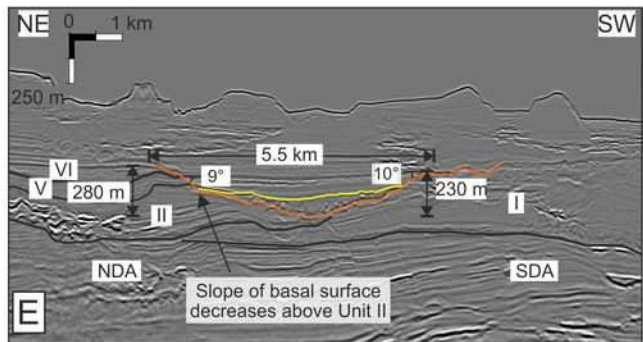
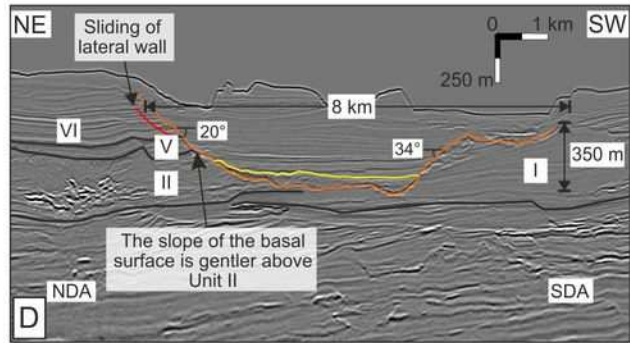
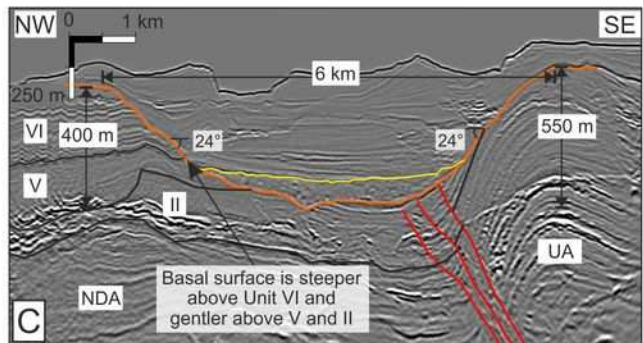
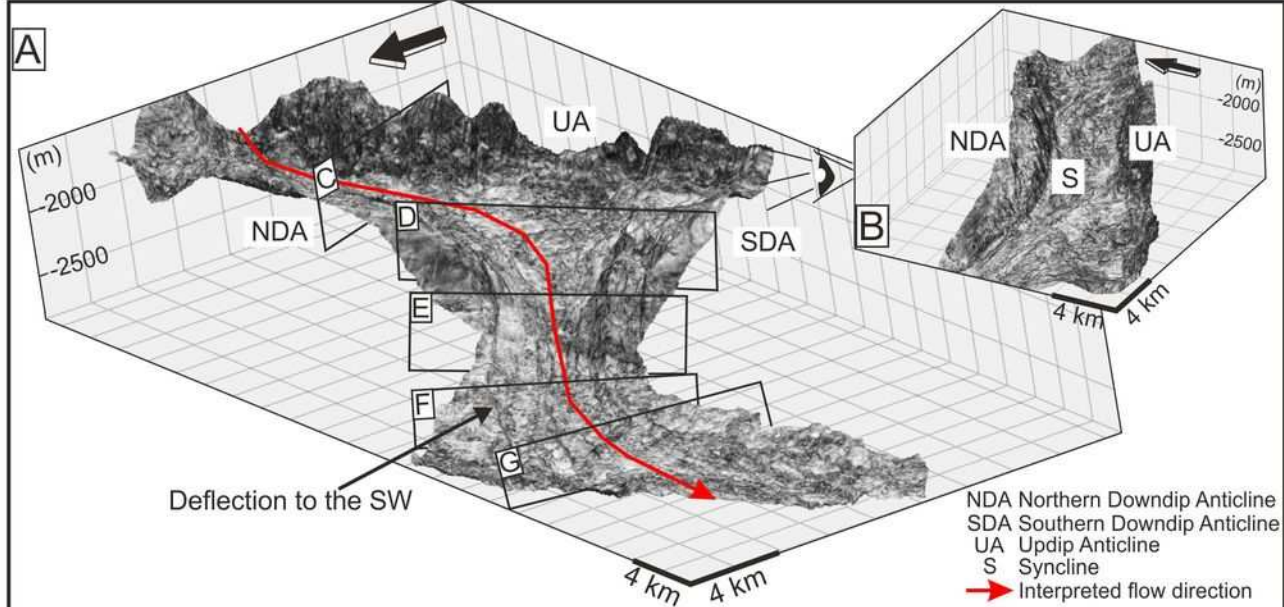


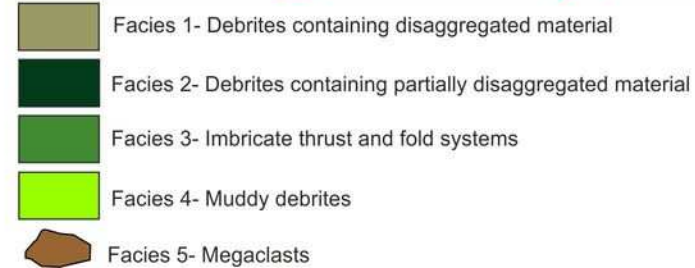
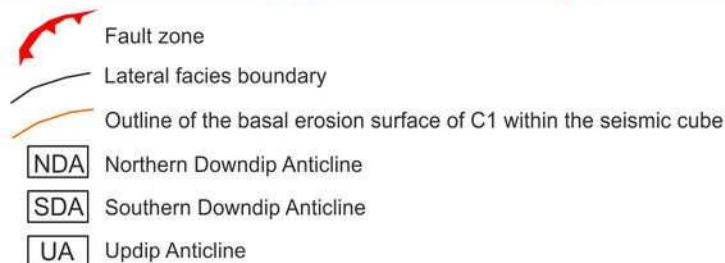
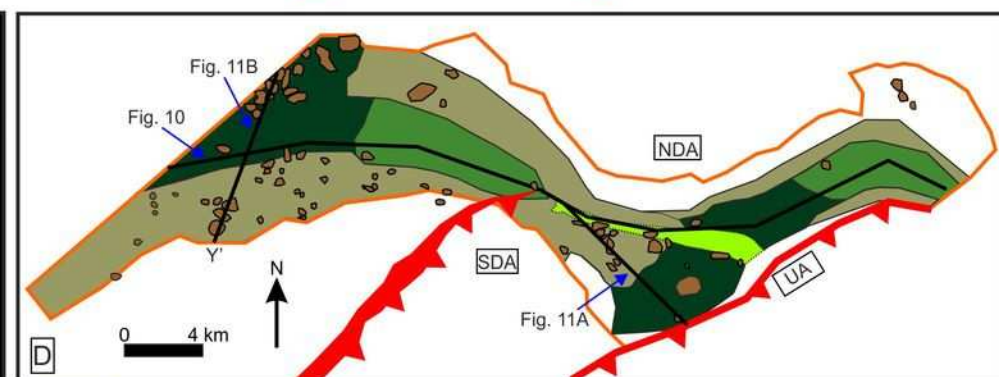
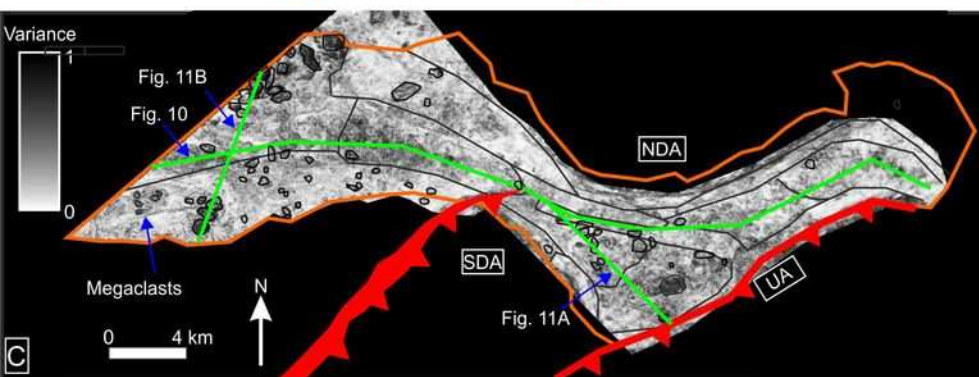
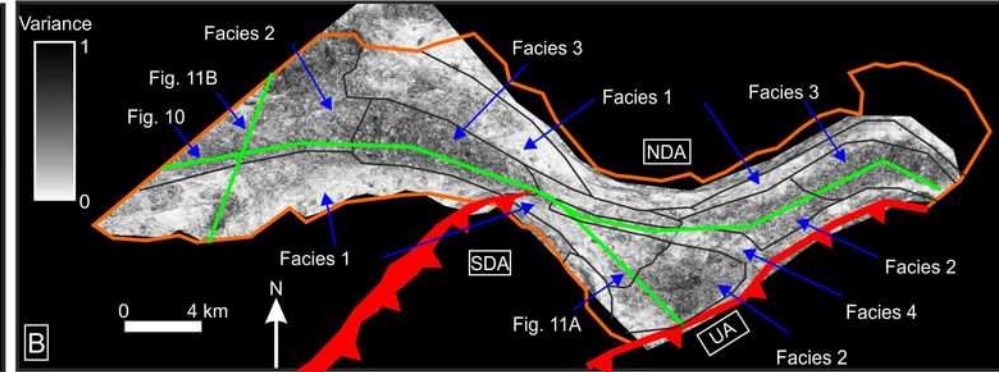
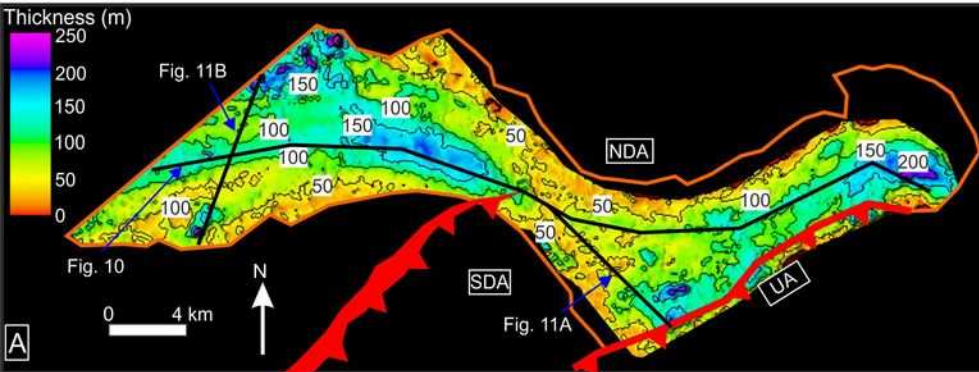


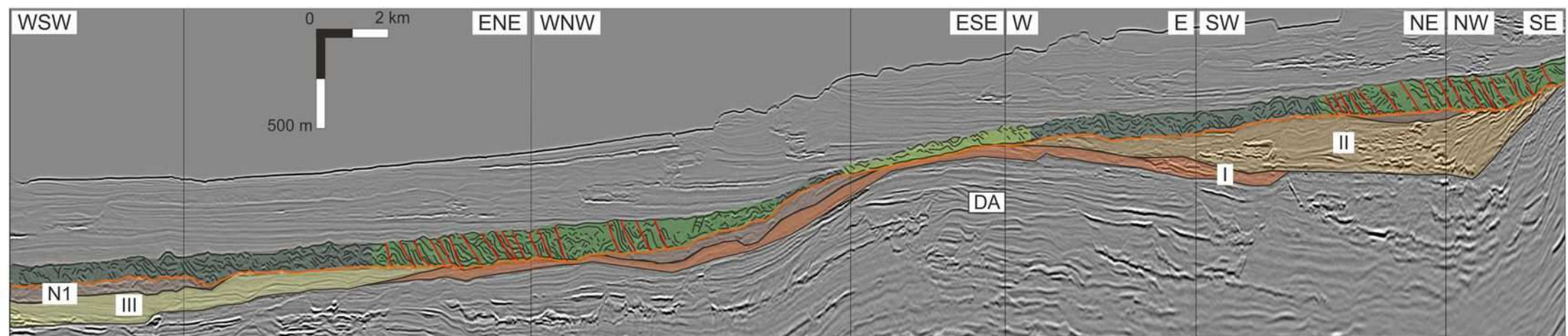
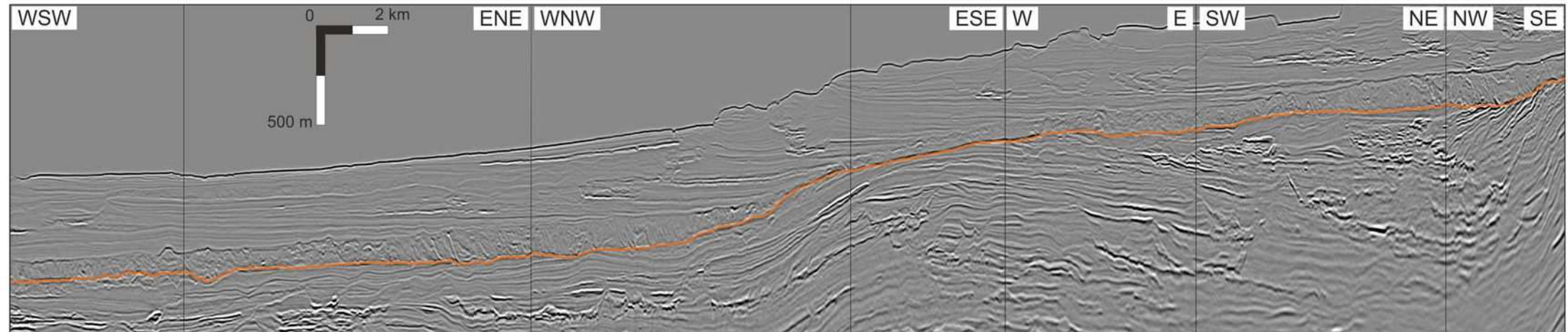














 Basal erosion surface of C1




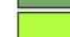
 Downdip Anticline

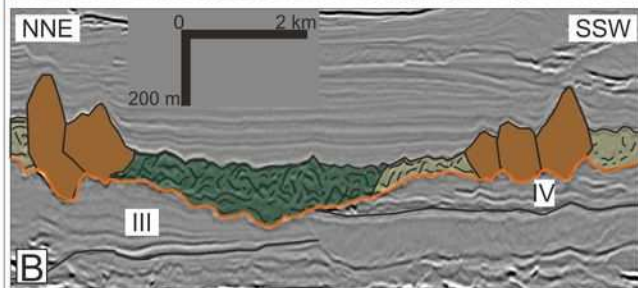
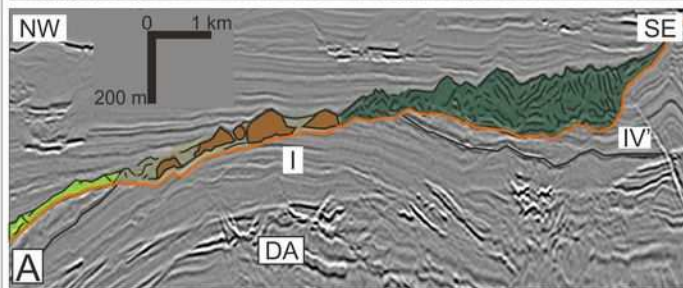
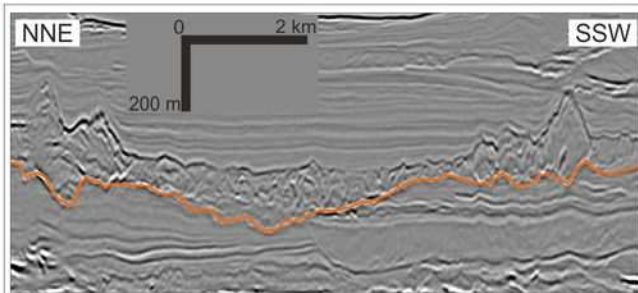
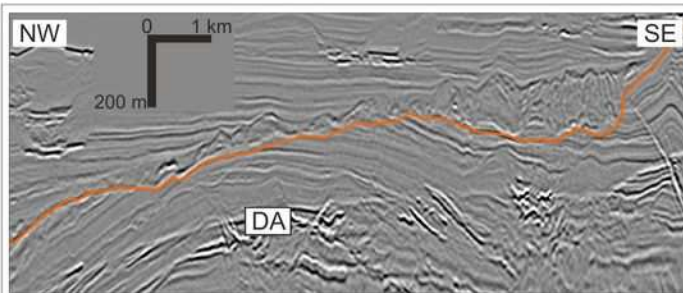
Substrate units








Younger ↑

IV	 MTCs
III	
II	
I	

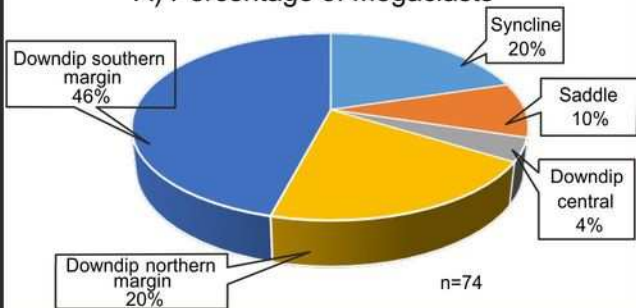
Seismic facies within C1

	Facies 1- Discontinuous chaotic reflections
	Facies 2- Semicontinuous variable-amplitude, folded reflections
	Facies 3- Thrust and fold systems
	Facies 4- Low amplitude, few internal reflections

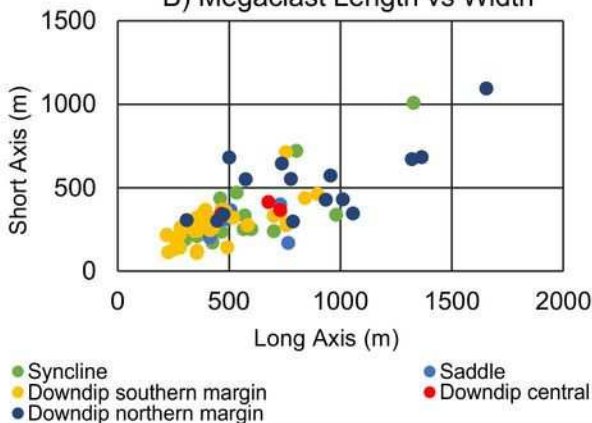


- | | | | |
|---|--|---|-----------------------------|
|  | Facies 1- Debrites containing disaggregated material |  | Facies 5- Megaclasts |
|  | Facies 2- Debrites containing partially disaggregated material |  | Basal erosion surface of C1 |
|  | Facies 3- Imbricate thrust and fold systems |  | Downdip Anticline |
|  | Facies 4- Muddy debrites | | |

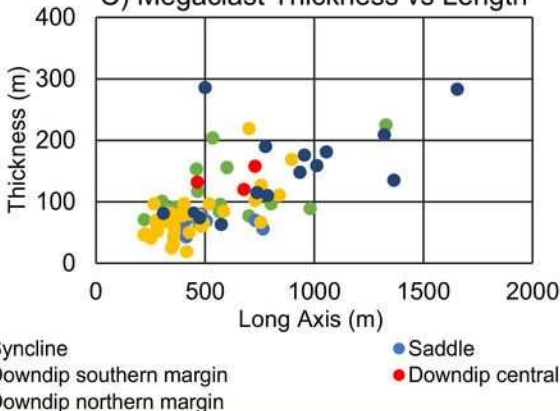
A) Percentage of Megaclasts

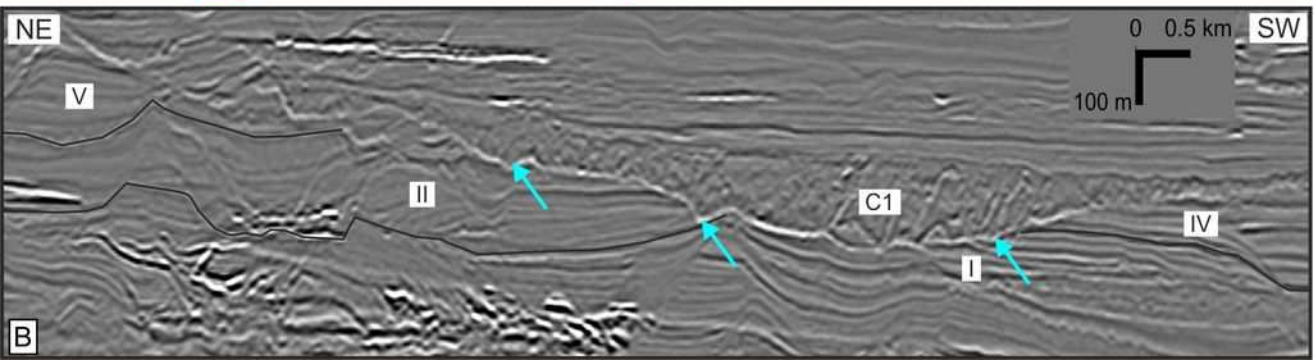
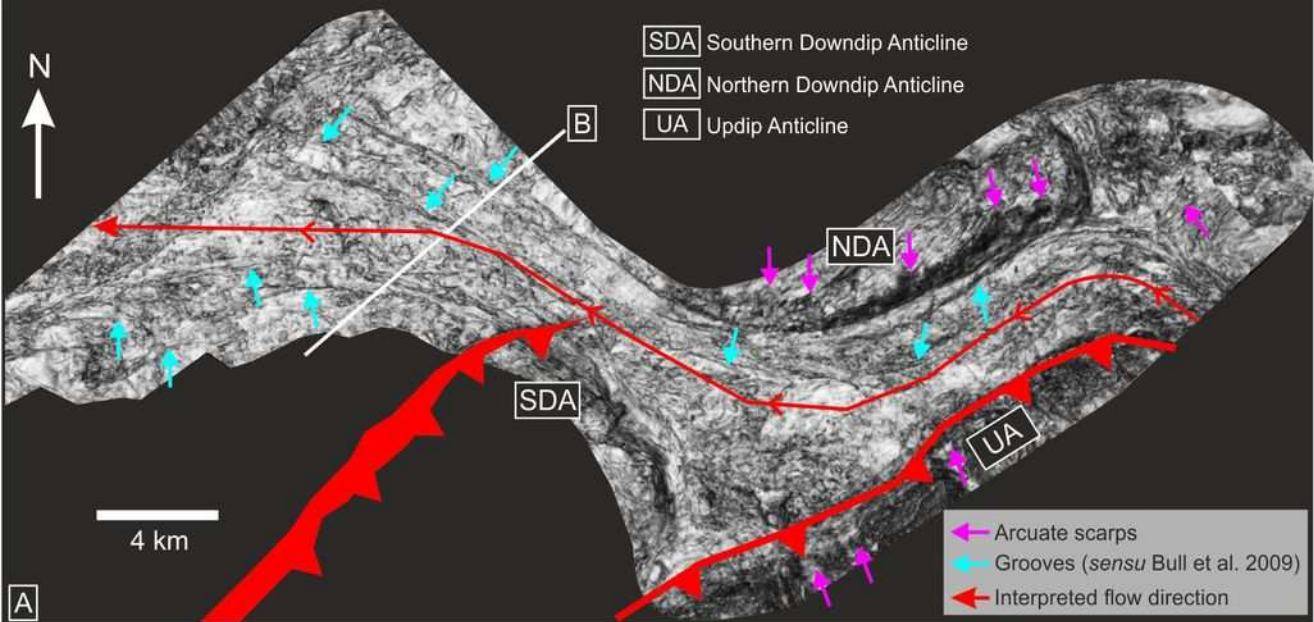


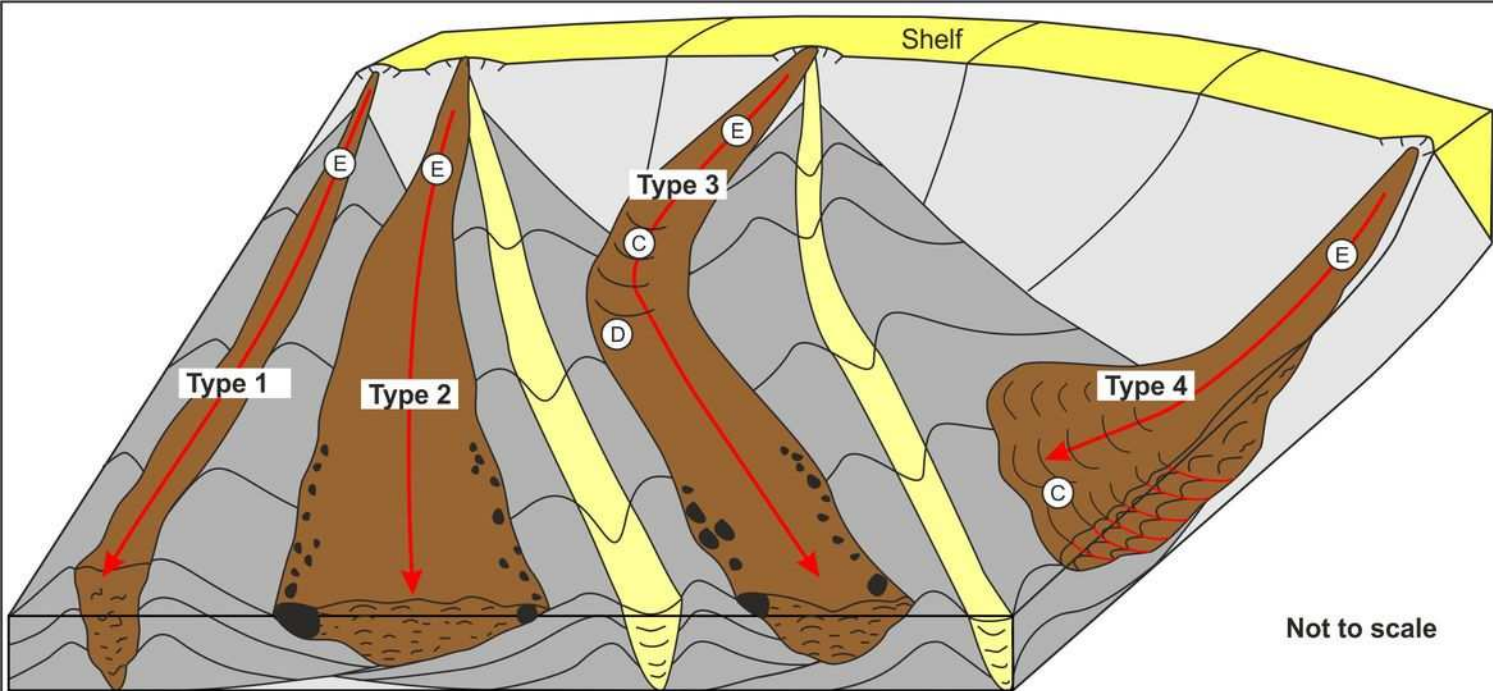
B) Megaclast Length vs Width



C) Megaclast Thickness vs Length







- External channel levees
- Channel-fill deposits
- MTCs
- Undifferentiated substrate
- Megaclasts

- Flow direction
- (C) Contractional deformation: imbricate thrust and fold systems
- (E) Erosion and bypass
- (D) Diversion

